Observations and Models of the Long-Term Evolution of Earth's Magnetic Field

Julien Aubert · John A. Tarduno · Catherine L. Johnson

Abstract The geomagnetic signal contains an enormous temporal range—from geomagnetic jerks on time scales of less than a year to the evolution of Earth's dipole moment over billions of years. This review compares observations and numerical models of the long-term range of that signal, for periods much larger than the typical overturn time of Earth's core. On time scales of 10^5–10^9 years, the geomagnetic field reveals the control of mantle thermodynamic conditions on core dynamics. We first briefly describe the general formalism of numerical dynamo simulations and available paleomagnetic data sets that provide insight into paleofield behavior. Models for the morphology of the time-averaged geomagnetic field over the last 5 million years are presented, with emphasis on the possible departures from the geocentric axial dipole hypothesis and interpretations in terms of core dynamics. We discuss the power spectrum of the dipole moment, as it is a well-constrained aspect of the geomagnetic field on the million year time scale. We then summarize paleosecular variation and intensity over the past 200 million years, with emphasis on the possible dynamical causes for the occurrence of superchrons. Finally, we highlight the geological evolution of the geodynamo in light of the oldest paleomagnetic records available. A summary is given in the form of a tentative classification of well-constrained observations and robust numerical modeling results.

J. Aubert (✉)
Bureau 459, Institut de Physique du Globe de Paris, 1 Rue Jussieu, 75238 Paris cedex 05, France
e-mail: aubert@ipgp.fr

J.A. Tarduno
Department of Earth and Environmental Sciences, University of Rochester, Rochester, USA
e-mail: john@earth.rochester.edu

C.L. Johnson
University of British Columbia, Vancouver, Canada
e-mail: cjohnson@eos.ubc.ca

1 Introduction

On time scales of 10^5–10^9 years, the geomagnetic field is dominantly dipolar in structure, in either its current (normal) or opposite (reverse) polarity. Global and regional variations in intensity and direction of the field over geological time provide insight into the evolution of the geodynamo, which in turn is governed by the thermochemical evolution of Earth's core. For example, the presence, strength and variability of the magnetic field during the Archaean can help elucidate the onset and early evolution of the geodynamo (Labrosse 2003; Tarduno et al. 2007; Nimmo 2007), and the associated thermal state of the mantle and core. Over time scales of 10^6 to 10^8 years, correlations among reversal rate, intensity, and temporal variability of the field during stable polarity periods may be diagnostic of the globally-averaged core-mantle heat flux and its spatial variations (Gubbins and Richards 1986; Larson and Olson 1991; Glatzmaier et al. 1999).

The Geocentric Axial Dipole (GAD) hypothesis, one of the fundamental tenets of paleomagnetism, states that the time-averaged magnetic field can be described by the field due to a dipole placed at the center of the Earth, and aligned with the Earth's rotation axis (Hospers 1951; Cox and Doell 1960; Opdyke and Henry 1969). Formulated in its modern form by Cox and Doell (1960), the GAD hypothesis was compatible with early understanding of the geodynamo as a homogeneous process, the time-average of which should display no or little symmetry-breaking. However, it was quickly acknowledged (Cox and Doell 1964; Hide 1970) that thermal control from a heterogeneous lower mantle could break such symmetries in the time-average. Persistent non-GAD structure in the historical (10^2 yr time scales) field (Gubbins and Bloxham 1985; Bloxham and Jackson 1989; Jackson et al. 2000), suggested that lateral variations in heat flux at the core-mantle boundary (CMB) could indeed influence the geodynamo in observable ways, and subsequently the search for deviations from the GAD in the paleomagnetic field has become an active topic of research (see reviews in Merrill and McFadden 2003; Johnson and McFadden 2007). Temporal variability in the magnetic field, typically characterized by the latitudinal variation in angular dispersion in direction or equivalent virtual geomagnetic pole (VGP) position has also been suggested to be diagnostic of the relative roles of equatorially symmetric or antisymmetric contributions to the geodynamo (McFadden et al. 1991), possibly reflecting the influence of long-term changes in core-mantle thermal conditions. The apparent preferred "longitude bands" for VGP paths during reversals has also been interpreted as a consequence of core-mantle interactions (Clement 1991; Laj et al. 1991; Costin and Buffett 2005).

In 1995, the emergence of numerical models of the geodynamo (Glatzmaier and Roberts 1995) allowed, for the first time, direct simulation of paleomagnetic observables. In a landmark study, Glatzmaier et al. (1999) investigated the effect of thermal conditions at the CMB on the predicted dipole moment and reversal rate. Subsequent studies have examined predictions for additional observables such as the time-averaged field morphology (Bloxham 2002; Olson and Christensen 2002), the power spectrum of variations in the dipole moment (e.g., Olson 2007), and latitudinal variations in VGP dispersion (Davies et al. 2008). Recent numerical dynamo modelling efforts have aimed to systematically explore the parameter space accessible to direct simulation (e.g. Christensen and Aubert 2006). Such studies allow quantification of the changes in dynamo properties that result from one or more changes in external forcing conditions.

The past decade has also seen significant improvements in paleomagnetic data sets. Such data are unlike their observatory or satellite counterparts in that typically it is not possible to recover the full field vector as a continuous function of time at any one location. Thus paleomagnetic data sets pertaining to a particular geological time interval

are usually heterogeneous in type (direction or intensity), and uneven in temporal and spatial coverage. Directional and intensity data sets spanning the past few million years have increased in quality, spatial distribution and temporal control (Johnson et al. 2008; Tauxe and Yamazaki 2007), allowing better assessment of global variations in magnetic field structure and strength (Valet et al. 2005; Johnson et al. 2008; Channell et al. 2009). Novel approaches to paleointensity determination utilizing new recorders including basaltic glass (Tauxe and Staudigel 2004) and single silicate crystals (Cottrell and Tarduno 1999) have led to increased scrutiny of the potential relationship between reversal rate and field strength (Tarduno et al. 2007, 2010). The ability to measure paleointensity on single silicate crystals hosting magnetic inclusions has also provided field strength estimates of the most ancient field between 3.2 and 3.45 Gyr Tarduno et al. (2007, 2010).

In this paper we review recent efforts in geodynamo modeling, specifically the parameter space and types of boundary conditions that can be captured in numerical simulations (Sect. 2). We outline the types of paleomagnetic observables that provide information on field behavior on time scales of 10^5 to 10^9 years (Sect. 3), and that can ultimately be used as tests of, or discriminants among, dynamo models. We discuss different aspects of field behavior that are amenable to comparisons of simulated and paleomagnetically-observed field behavior as follows. We compare paleomagnetically-derived models for the global time-averaged field (Sect. 4.1) with those predicted by simulations (Sect. 4.2). We focus in particular on non-GAD structure in the paleomagnetic field, and the extent to which such structure in simulations depends on the core-mantle boundary heat flux conditions imposed, and other critical parameters, such as the Ekman number. Because our interest here is in longitudinal, as well as latitudinal, structure in the field we restrict our discussion to paleofield models spanning only the past few Myr, the time period over which uncertainties in plate motion corrections are smaller than the signals of interest in the field. In addition these types of field models have, to date, been primarily derived from paleomagnetic directional data from igneous rocks. However, continuous records available from deep sea sediments provide another important constraint on paleo-field behavior over the past 2 Myr, as individual time series of relative paleointensities from different locations can be combined to provide a global model for temporal variations in the axial dipole moment, allowing investigation of the power spectrum of dipole moment variations. We compare power spectra (Sect. 5.1) obtained from two such global models with the corresponding predictions from dynamo simulations (Sect. 5.2). We then turn our attention to statistical properties of the field over time scales of 0–195 Myr (Sect. 6), constrained mainly by paleomagnetic data from igneous rocks. Specifically, we examine the dispersion in field direction or equivalent VGP positions (Sects. 6.1 and 6.2), the mean intensity of the field (Sect. 6.3), and correlations among these properties and reversal rate. We do not examine the process of reversals in detail as these are discussed elsewhere in this volume. We discuss the influence of various parameters in numerical simulations on predictions for VGP dispersion, and on relationships among intensity, reversal rate and PSV. In Sect. 7 we discuss the longest time scales, including the onset and early evolution of the field. We review the challenge of obtaining observations for Archean ages and new approaches that have yielded paleofield strength data (Sect. 7.1). We then discuss modelling of the geodynamo of these billion year time scales (Sect. 7.2) and compare the modelling results with observations (Sect. 7.3).

Throughout the paper, we discuss the sensitivity of the predictions from simulations to the boundary conditions and numerical parameter space that can presently be explored. We examine how heterogeneous boundary conditions such as heat flux and their globally averaged values affect the presence or absence of rotational or equatorial symmetries in field behavior, and the long-term evolution in magnetic field strength. Throughout, we point out

agreement and disagreement between data and model results, and suggest ways in which both approaches can improve our understanding of the geodynamo.

2 Numerical Dynamo Models

2.1 Formalism

The field of numerical dynamo modelling has reached maturity through the availability of several computer codes, that have been checked to yield similar results through the Dynamo Benchmark initiative (Christensen et al. 2001). Here we provide an attempt to outline the general formalism of most situations which have been encountered in the recent literature.

We consider an electrically conducting, incompressible Boussinesq fluid in a self-gravitating spherical shell between radii r_i and r_o. The shell is rotating about an axis $\mathbf{e}_z$ with an angular velocity Ω, and is convecting thermally and chemically. The aspect ratio $\chi = r_i/r_o$ is a control parameter of the model. Buoyancy sources which contribute to convection in the Earth's core are of thermal (arising from the secular cooling of the core) and chemical (consecutive to the inner core freezing and associated release of light elements) types (Braginsky and Roberts 1995; Lister and Buffett 1995). Most dynamo codes use a single type of buoyancy, which can be generically described as a density anomaly, or co-density C. Indeed, as the two buoyancies are not thought to have mutually opposing effects, double diffusive convection is not expected. If we define the deviation temperature field T' and light element mass fraction field ξ' with respect to the isentropic temperature and well-mixed mass fraction, the co-density field C can be written (Braginsky and Roberts 1995):

$$C = \alpha\rho T' + \Delta\rho\xi' \tag{1}$$

Here α is the thermal expansion coefficient, ρ is the fluid density, and $\Delta\rho$ is the density difference between the light components that contribute to chemical convection and pure iron. Assuming turbulent diffusivity, and hence a single diffusivity for both the thermal and chemical convection (Braginsky and Roberts 1995), a single transport equation for the co-density C can be written, which is solved numerically in a dimensionless form, together with the magnetic induction equation for the solenoidal magnetic field $\mathbf{B}$ in the magnetohydrodynamic approximation, and the Navier-Stokes and thermo-chemical transport equations for the incompressible velocity field $\mathbf{u}$, and pressure P:

$$\frac{\partial \mathbf{u}}{\partial t} + \mathbf{u} \cdot \nabla\mathbf{u} + 2\,\mathbf{e}_z \times \mathbf{u} + \nabla P = Ra_F \frac{\mathbf{r}}{r_o} C + (\nabla \times \mathbf{B}) \times \mathbf{B} + E\nabla^2\mathbf{u} \tag{2}$$

$$\frac{\partial \mathbf{B}}{\partial t} = \nabla \times (\mathbf{u} \times \mathbf{B}) + \frac{E}{Pm}\nabla^2\mathbf{B} \tag{3}$$

$$\frac{\partial C}{\partial t} + \mathbf{u} \cdot \nabla C = \frac{E}{Pr}\nabla^2 C + 3\beta \tag{4}$$

$$\nabla \cdot \mathbf{u} = 0 \tag{5}$$

$$\nabla \cdot \mathbf{B} = 0 \tag{6}$$

Here $\mathbf{r}$ is the radius vector. Time is scaled by the inverse of the rotation rate Ω^{-1}. Length is scaled by the shell gap $D = r_o - r_i$. Velocity is scaled by ΩD. Magnetic induction is scaled

by $(\rho\mu)^{1/2}\Omega D$, where ρ is the fluid density and μ the magnetic permeability of the fluid. The Ekman number E, magnetic Prandtl and Prandtl numbers Pm and Pr are defined as:

$$E = \frac{\nu}{\Omega D^2} \tag{7}$$

$$Pm = \frac{\nu}{\lambda} \tag{8}$$

$$Pr = \frac{\nu}{\kappa} \tag{9}$$

Here ν, λ are respectively the viscous and magnetic diffusivities of the fluid. Usually mechanical boundary conditions are of the rigid (no-slip) type. The magnetic boundary condition at the outer (core-mantle) boundary is insulating, and at the inner (inner core) boundary is conducting. This latter condition is often replaced with an insulating condition, as a number of simulations show (e.g. Wicht 2002) that the influence of a conducting inner core on various properties of the solution is weak.

Modelling the long-term properties of the geodynamo requires special attention to be given to the thermal boundary condition. A thermally heterogeneous mantle should extract a spatially variable heat flow from an essentially isothermal core. For that reason, the outer boundary condition constrains the mass anomaly flux (which reduces to a thermal flux, due to an assumed absence of chemical flux to the mantle):

$$f(r_o) = -\kappa \nabla C \cdot \mathbf{r}/r_o \tag{10}$$

Here κ is the thermo-chemical diffusivity of the fluid. The outer boundary mass anomaly flux is decomposed into an homogeneous part f_o and an heterogeneous part proportional to a single harmonic pattern, or, more realistically, to lower mantle seismic shear wave tomography, which is assumed to provide a proxy for heat flow anomalies (Glatzmaier et al. 1999). A typical tomographic map is shown in Fig. 1. The ratio $q^* = \Delta f/2f_o$ between the zero-to-peak heat flow variation and the average heat flow measures the degree of heterogeneity. The effect of single harmonic components has also been studied (Olson and Christensen 2002; Willis et al. 2007).

A sensible, and frequently used (e.g. Olson and Christensen 2002; Willis et al. 2007) boundary condition at the inner boundary is one of constant co-density. Recently it has been argued (Aubert et al. 2008b, supplementary material) that this condition provides an approximate description (within the framework of the Boussinesq approximation) of a surface which evolves at its melting temperature (see also Anufriev et al. 2005).

The co-density is scaled with $f_o/D\Omega$. The Rayleigh number based on mass anomaly flux, Ra_F, which appears in (2) is therefore defined as:

$$Ra_F = g_o f_o/\rho \Omega^3 D^2 \tag{11}$$

Fig. 1 Map of the imposed mass anomaly flux at the outer boundary, here proportional to velocity anomalies from seismic shear model SB4L18 (Masters et al. 2000). *Red* (*blue*) regions extract more (less) heat from the underlying core
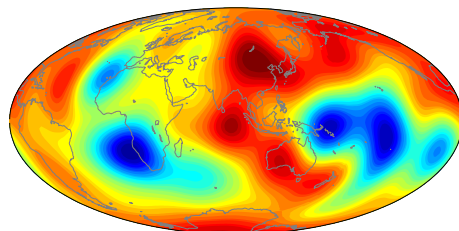
Table 1 Dimensionless numbers of dynamo models. The Earth estimates can be found e.g. in Christensen and Aubert (2006)

Input parameter	Definition	Meaning	Model	Earth
Ekman	E	viscous force/Coriolis force	3.10^{-4}–3.10^{-6}	10^{-15}
Flux Rayleigh	Ra_F	buoyancy	10^{-9}–10^{-3}	10^{-13}
magnetic Prandtl	Pm	viscosity/mag. diffusivity	0.1–10	10^{-6}
Prandtl	Pr	viscosity/thermochem. diffusivity	0.1–10	?
aspect ratio	χ	geometry	0–0.35	0.35 today
flux heterogeneity	q^*		0–1	?

The term β in (4) describes an Earth system that is slowly cooling on geological time scales. In this case the basic state over which the Boussinesq system is considered has a decreasing temperature and increasing light element mass fraction, while the Boussinesq system itself is statistically stationary. In some studies (Gubbins et al. 2007; Willis et al. 2007; Sreenivasan and Gubbins 2008), the Rayleigh number is defined through β instead of f_o, but the formalism is otherwise equivalent. In Sreenivasan and Gubbins (2008), the volumetric distribution of β is furthermore employed to simulate the presence of an applied stably stratified fluid layer at the top of the core.

Table 1 shows the parameter space that has been studied in recent numerical dynamo modelling. It should be kept in mind that due to computational limitations, all accessible numerical dynamo simulations operate in a parametric regime still very far from that of Earth's core. In particular, the Prandtl numbers, or ratios between diffusivities, are both close to one, and the Ekman number is much too high. However, the fact that numerical dynamos yield a long-term, and large scale outcome which is remarkably similar to the geomagnetic field is not as surprising as it may seem, given the parameter disparity. Indeed, as we will see below, numerical dynamos perform a correct modelling of magnetic induction: the magnetic Reynolds number, measuring the ratio of the advection time scale and the magnetic dissipation time scale, has the amplitude 100–1000 in the models versus about 1000 for the Earth's core. However, numerical modelling fails at describing the details of the intense hydrodynamic turbulence: the hydrodynamic Reynolds number is up to 1000 in models versus 100 million in the Earth's core. Whether a correct modelling of the hydrodynamic turbulence is needed to describe the large scales, and long time scale behavior of the magnetic field is a topic of active research. One assumption is that owing to the very large magnetic diffusivity in the Earth's core, these scales will be mostly sensitive to the corresponding scales of the velocity field, and not to the faster, smaller-scale details of the turbulence. This assumption has been partly justified by a systematic analysis of morphological similarities between the output of numerical dynamos and the geo- and paleomagnetic field (Christensen et al. 2010), where it was shown that two main parameters determining the resemblance of geodynamo models to the actual field are the magnetic Reynolds number (controlling how well the induction is modelled as seen above), and the magnetic Ekman number $E_\lambda = E/Pm = \lambda/\Omega D^2$. This last number is the ratio of the length of a day to the magnetic diffusion time, and can be seen as an indicator of how strongly the Coriolis force constrains scales in the velocity field which are large in space and long in time with respect to typical magnetic diffusive time scales. The dynamo process at work in numerical dynamos may thus bear some similarity with the process present in planetary cores as long as the magnetic Reynolds number approaches a value of 1000 and the magnetic Ekman number is low enough (the target planetary value is 10^{-9} and numerical dynamos models go

as low as about 10^{-6}). The philosophy of numerical dynamo modelling is then to illustrate the physical similarity between models and natural objects by identifying robust trends supported by reasonable underlying physical considerations, and their corresponding scaling laws (e.g. Christensen and Aubert 2006).

2.2 Time Scales in Numerical Simulations

When examining the behavior of the paleomagnetic field, the question of the time interval over which we should examine numerical simulations (for both their time-averaged properties and their temporal variability) naturally arises. As it is understood in the present paper, such time intervals should be sufficiently long to average out core dynamics, but sufficiently short for the external influence of the mantle to be considered static in time. An upper bound on such a time interval is determined by the mantle and is given by the typical turnover time for mantle convection, or about 100 Myr. This is also the typical time for the growth of a few tens of kilometers of the inner-core boundary (Aubert et al. 2008b). A lower bound is the typical core overturn time D/U, which is about 100 years if $D = 2200$ km and a typical velocity $U = 0.5$ mm/s is extracted from surface core flows obtained from the secular variation of the geomagnetic field (Bloxham and Gubbins 1987; Hulot et al. 2002). Obviously, averaging over a large number of core overturn times is needed to truly average out core dynamics, so that a target of 100 kyr to 1 Myr (1000–10000 overturns) would probably represent the ideal time averaging window (Olson and Christensen 2002; Christensen and Olson 2003). In one of the fundamental time units used in numerical dynamo modelling, the magnetic diffusion time $D^2/\eta \approx 115$ kyr, this translates into a few units. It should however be kept in mind that the magnetic Reynolds number $Rm = UD/\lambda$, which can be seen as a measure of the turnover frequency on the magnetic diffusion time scale, and hence the fundamental frequency of magnetic variability, is usually lower in numerical dynamos (100–500) than in the Earth, where a value of 1000 is favoured (Christensen and Tilgner 2004). As a result, and in order to correct for this discrepancy, it is best to express the required time averaging time in units of the turnover. Similar requirements are reached by paleomagnetic estimates of the required time averaging window (e.g. Merrill and McFadden 2003)

3 Paleomagnetic Data Sets

Paleomagnetic observations useful to global magnetic field studies over time scales of 10^4 years and longer comprise measurements of direction (declination, D, and inclination, I) and/or intensity, $|B|$ from igneous or sedimentary rocks. Igneous rocks, specifically lava flows or thin dikes, provide intermittent or spot readings of the paleofield, whereas sedimentary sections and deep-sea sediment cores, provide continuous time series of observations. Typically, the full vector field is not available for a given place and time. Lava flow data are (D, I) pairs, sometimes accompanied by estimates of absolute paleointensity. Deep-sea sediment cores typically provide some combination of measurements of I, relative or absolute D, and relative intensities that must be scaled to give an absolute paleointensity (Valet 2003; Tauxe and Yamazaki 2007). Temporal control of both sediment cores and lava flow data sets is limited—in the former case variations in sedimentation rate, and establishing an independent chronology for the core is challenging, in the latter case only a small fraction of existing data sets have radiometric dates on the specific flow or dike being measured. These issues, together with uneven spatial coverage mean that data sets of sufficient quality and

quantity hamper investigations of global paleomagnetic field behavior. A complete review of data sets used in such studies is beyond the scope of this paper (see reviews in Johnson and McFadden 2007; Tauxe and Yamazaki 2007); however over the past decade much effort has gone into improving such data sets, in particular for the 0–5 Myr interval. Recent global compilations of lava flow directions and of paleointensity are reported in Johnson et al. (2008) and Tauxe and Yamazaki (2007) respectively. Such 0–5 Myr data sets can be used to explore both latitudinal and longitudinal variations in field structure because errors in plate motion corrections are less than the signals of interest in the time-averaged field direction.

For time intervals of 10^7 to 10^9 years, the dipole axis cannot be assumed to be the geographic axis as plate motion will have caused large changes in site location relative to the present-day. Some studies of paleomagnetic data on these time scales have called for large nondipole fields for Mesozoic-Paleozoic (Van der Voo and Torsvik 2001; Torsvik and Van der Voo 2002) and Paleozoic times (Kent and Smethurst 1998) but these inferences tend to conflict with assessments based on geologic data (e.g. Evans 2006) and data in each study can be interpreted as reflecting uncertainties related to site position and/or magnetization process (e.g. Tauxe and Kent 2004).

After defining site latitude, progress in the defining the nature of the past field must address the ever-present possibility of contamination of the data by natural or laboratory induced processes. These effects, which include weathering of rocks and alteration associated which subsequent geologic events, can transform thermoremanent magnetizations into chemical remanences. Even smaller scale changes (e.g. formation of clays) can result in laboratory artifacts related to the formation of new magnetic minerals (Tarduno and Smirnov 2004). These issues affect paleointensity data more than directional studies because the former require measurements in the presence of an applied field to gauge past field strength (see discussion in Tarduno et al. 2006).

There has been an increased awareness of the potential problems in paleointensity measurements, and this has led to rigorous laboratory tests to check for natural and laboratory alteration, new techniques for paleointensity determination, and a search for magnetic carriers that are superior to whole rock samples of igneous rocks. We will focus on results from one of these new recorders—single silicate crystals hosting magnetic inclusions (Cottrell and Tarduno 1999)—the measurement of which has been made possible by advances in DC SQUID magnetometers for paleomagnetism. These have been applied to estimate field strength during mixed polarity intervals and superchrons (Tarduno and Cottrell 2005) as well as the field strength of the ancient dynamo (Tarduno et al. 2010). These studies provide a convenient data set for assessing current progress, comparing data with models, and pointing the way for future studies.

4 Morphology of the Time-Averaged Field

4.1 Paleomagnetic Field Models, 0–5 Myr

Studies of the time-averaged paleomagnetic field (TAF) have typically dealt separately with the mean virtual axial dipole moment (VADM) derived from measurements of paleointensity and the field morphology derived from measurements of direction. Note that in 0–5 Ma paleointensity studies, VADM is typically used, cf. VDM for the ancient field (Sects. 6.4.3 and 7.1), since for 0–5 Ma the mean dipole axis can be assumed to be the geographic axis, as the site paleolatitude is only minimally different from present latitude. We focus on directional data here, since they are more numerous, and are currently more appropriate for

investigations of non-GAD structure in the field. Models that can examine variations in both latitudinal and longitudinal structure in the TAF (and in paleosecular variation, PSV) are limited to the past 5 Myr, and the best data coverage is for the Brunhes (0–0.78 Myr) and Matuyama (0.78–2.5 Myr) chrons.

Small departures of the TAF from GAD were evidenced in early paleomagnetic studies (Opdyke and Henry 1969; Wilson 1970) as dominantly negative inclination anomalies with maximum magnitudes at low latitudes of a few degrees. A large number of studies followed in which this latitudinal structure for sediments and/or lava flows was described by low degree zonal spherical harmonic terms (Merrill and McElhinny 1977; Merrill et al. 1996; Johnson and McFadden 2007). Typically, the dominant term in such studies is the axial quadrupole (g_2^0) term, whose magnitude for normal polarity periods (Brunhes, Gauss) is 2%–5% of g_1^0; with a smaller axial octupole (g_3^0) term whose sign and magnitude varies among different studies depending on the data set examined. A small g_3^0 contribution— approximately 2% of g_1^0—is expected because of bias incurred due to the absence of intensity data in such studies. Asymmetries between normal and reverse polarity TAF structure were observed with a greater departure from GAD for reverse polarity periods. Since the latter observation is not predicted by dynamo theory, the asymmetry was interpreted to reflect heterogeneous core-mantle boundary conditions, or simply poor data quality (Merrill et al. 1996). High quality paleomagnetic data sets for 0–5 Myr collected and compiled over the past decade allow investigation specifically of the Brunhes normal and Matuyama reverse polarity periods and these new data support previous observations of normal/reverse asymmetry (Fig. 2).

Geographical structure (both longitudinal and latitudinal variations) in the TAF has been modeled using previous compilations of lava flow and sediment data sets and regularized non-linear inversion techniques (Gubbins and Kelly 1993; Johnson and Constable 1995, 1997; Kelly and Gubbins 1997). Features similar to those observed in historical field models, notably high latitude flux bundles and persistent structure in the Pacific region are observed (Fig. 3), although different views exist as to the robustness of such structure (see review in Johnson and McFadden (2007)).

In Fig. 3 we show a new TAF model for the Brunhes generated using the modeling approach of Johnson and Constable (1995, 1997), but including only the regional compilations and high quality data reported in Johnson et al. (2008). The model is motivated by the observations of regional differences in the mean inclination anomaly at 20° latitude (Lawrence et al. 2006) and regional variations in TAF directions from new data reported (Johnson et al.
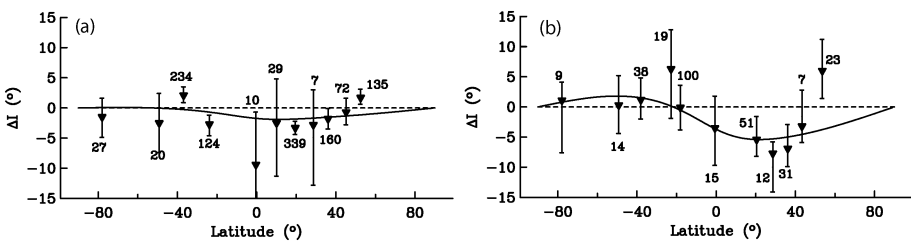

Fig. 2 Inclination anomaly versus latitude (*triangles*) with 95% confidence intervals (*error bars*) for latitudinally binned lava flow data for (**a**) Brunhes, (**b**) Matuyama periods. *Solid black lines* are the best-fit 2-parameter zonal spherical harmonic models (from Johnson et al. 2008). Numbers of data at each location are given. Spherical harmonic coefficients for the best-fit models are (**a**) Brunhes: $g_2^0 = 2\% \, g_1^0$, $g_3^0 = 1\% \, g_1^0$, and (**b**) Matuyama: $g_2^0 = 4\% \, g_1^0$, $g_3^0 = 5\% \, g_1^0$
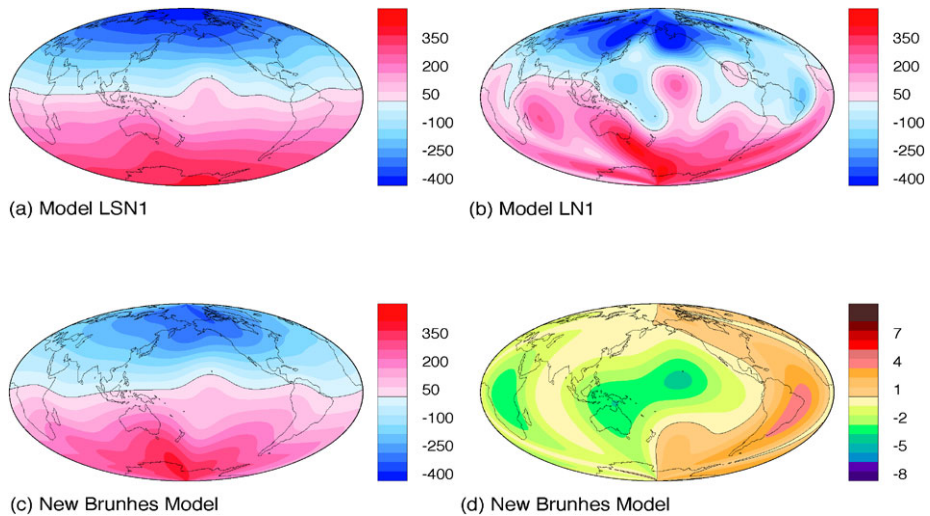
Fig. 3 B_r at the CMB in μT for various TAF models—(**a**) LSN1 based on lavas and sediments (Johnson and Constable 1997), (**b**) LN1 based on lavas (Johnson and Constable 1995), (**c**) Brunhes TAF model using only data reported in Johnson et al. (2008). (**d**) Inclination anomalies in degrees at the surface predicted by the model in (**c**)

2008). The model includes 18 pairs of time-averaged declination and inclination measurements (i.e., data from 18 locations worldwide). The normalized root-mean-square misfit of a model to the data is given by $\sum_{i=1}^{N}[(d_{obs}^i - d_{pred}^i)/\sigma_i]^2$, where d_{obs}^i and d_{pred}^i are the i'th observation and model prediction respectively, σ_i is the associated uncertainty in the observation, and N is the number of data. We fit the data to the 95% confidence limit on the expected value of χ^2 (a value of 1.3). For a GAD model the normalized RMS misfit is 2.1, i.e., a GAD model does not fit the observations at the 95% confidence level. The variance reduction of the TAF model in Fig. 3 compared with that of a GAD model is over 60%. (See Johnson and Constable 1995, 1997 for a complete description of data error assignment, choice of misfit level, and inversion procedure.) The data set of Johnson et al. (2008) is not global in coverage, in that e.g., regional compilations from Europe that were included in previous TAF modeling studies have not yet been updated and are hence excluded, since the intention here is to use only high quality data. Note that even in the absence of such data sets the updated model shows substantial longitudinal structure, in particular persistent structure beneath Hawaii, and increased radial flux at high latitudes over N. and S. America, N. Zealand and Japan, regions with greatly improved data coverage in the new data set. Future modeling efforts can include not only additional high quality directional data, but also new absolute paleointensity data from igneous rocks, and continuous time series of inclination, relative declination and relative paleointensity from deep sea sediment cores.

4.2 Predictions from Numerical Simulations

Using a numerical dynamo model influenced by a boundary heat flow heterogeneity consisting of a single degree 2, order 2 harmonic, the dominant signal from seismic tomography maps such as presented in Fig. 1, Bloxham (2002) first reported core-mantle boundary magnetic flux bundle concentrations at specific geographic longitudes for a 360 kyr time-average of the field. The locations of these flux bundles agreed with those observed in the present

(Hulot et al. 2002), historical (Jackson et al. 2000), and paleomagnetic (Kelly and Gubbins 1997; Johnson and Constable 1995) fields, that is, one patch beneath America and one beneath Siberia in the Northern hemisphere, with corresponding patches at roughly the same longitude in the southern hemisphere. Inspection of the model revealed that the longitude of these persistent magnetic patches were close to the regions of high heat flow extracted by the mantle. A systematic analysis of the same type of models was subsequently carried out by Olson and Christensen (2002), using full tomographic heat flow patterns in addition to single harmonics and including a parameter space exploration of the magnitude of the heterogeneity. They were able to confirm the existence of persistent patches (Fig. 4), and outlined the mechanism for their creation: the boundary heat flow heterogeneity maintains a long-term thermal wind; at the center of the cyclonic gyres of this thermal wind, a converging flow (Olson et al. 1999) concentrates the magnetic field into permanent bundles. It should be noted that the longitude of these bundles does not necessary coincide with that of the main features of imposed heat flow. Indeed, the thermal wind is sensitive to temperature gradients, while only the heat flow is imposed. Advection of the thermal field by the underlying convection can therefore shift the main long-term features of the temperature field with respect to these of the imposed heat flow. However, as this shift is generally not large, there were several subsequent reports of agreement between the longitudes of modeled and observed persistent flux bundles (Gubbins et al. 2007; Davies et al. 2008; Aubert et al. 2008b, see also Fig. 4) and even a possible connection with deeper core structure, such as the seismically-inferred hemispherical heterogeneity of the inner core (Aubert et al. 2008b). However, Fig. 4 also shows that the agreement between flux bundle location and geomagnetic data can also be questionable. (Olson and Christensen 2002) showed that while northern hemisphere magnetic patches from simulations coincide reasonably with their observed counterparts (again, one patch beneath America and one beneath Siberia), the southern hemisphere shows a patch that is harder to reconcile with geo- and paleomagnetic data.
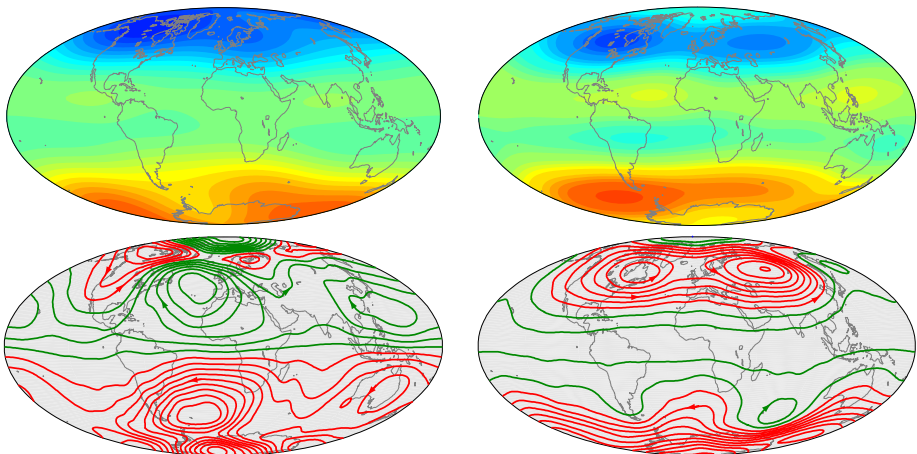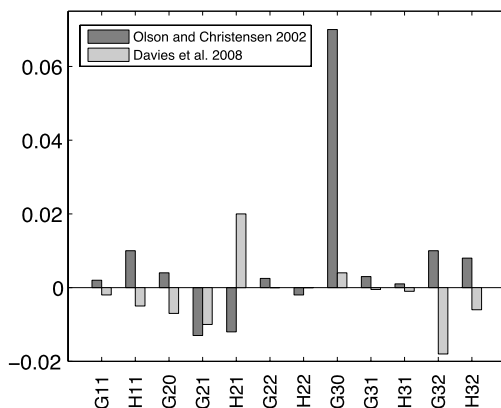

Fig. 4 *Top*: time average magnetic field, and *bottom*: streamlines of the time average flow below the core-mantle boundary (*red lines* in the northern hemisphere denote cyclonic (anticlockwise) gyres, see *arrows*), from the "tomographic" case of Olson and Christensen (2002) (*left column*, $Ra_Q = 6.9\ 10^{-5}$), and the case in Aubert et al. (2008a) (*right column*, $Ra_Q = 2.0\ 10^{-4}$). Other parameters for both cases are $E = 3\ 10^{-4}$, $Pr = 1$, $Pm = 2$, $q^* = 0.5$, $\chi = 0.35$. Note the coincidence between cyclonic gyres and magnetic flux concentration

More recently, Davies et al. (2008) have discussed predicted inclination and declination anomalies for a series of models for different q (η in their paper). They show that dynamos with strong lateral heterogeneity result in locked features in the field, in particular large longitudinal variations in inclination anomaly, somewhat similar to those observed in paleomagnetic data, but whose peak-to-peak amplitudes are much larger than observed from data. Such locked dynamos give longitudinally-averaged inclination anomalies that are dominantly positive in the northern hemisphere, in contrast to observations (Fig. 2). Interestingly, dynamo solutions with weaker lateral heterogeneity give latitudinal variations in inclination anomaly qualitatively more like those observed from Matuyama-aged paleomagnetic data (see Davies et al., Fig. 2).

Studies of mantle control on the time averaged field have also reported the low degree and order Gauss coefficients of the field (Olson and Christensen 2002; Davies et al. 2008). Figure 5 synthesizes the results found by two groups. The Gauss coefficients are normalized respectively to the value of g_{10}. (Absolute paleointensity of the field will be studied separately in Sect. 6.3.) Imposing a heat flow heterogeneity at the outer boundary populates the spectrum of the time average field significantly, as expected. However, differences in the forcing Ra_F, in the boundary heterogeneity q^* result in striking contrast between the models of Olson and Christensen (2002) and Davies et al. (2008). As reported in Sect. 4.1, most paleomagnetic studies find that the dominant non-GAD terms are g_2^0 and g_3^0. Typically, g_2^0 is the largest contribution, with a magnitude of 2% to 5% of g_1^0 for normal polarity periods during the past 5 Myr. Both numerical models fail to predict an axial quadrupole as strong as that inferred from inclination anomalies. On the time-average, the equatorial symmetry of numerical dynamos is not broken in models with homogeneous boundary conditions (Olson and Christensen 2002), though Bouligand et al. (2005) report a statistically significant quadrupole component present in a time average of the Glatzmaier and Roberts (1995) dynamo model. Olson and Christensen (2002) further showed that the axial quadrupole component is crucially sensitive to the amount of equatorial asymmetry present in the imposed heterogeneous heat flow condition. It is therefore tentative to speculate that the heterogeneous conditions which force the actual Earth system have a stronger content in equatorially asymmetric signal than that present in the map of Fig. 1. In contrast, obtaining an axial octupole in the numerical models which is at least as strong as the paleomagnetic inference seems feasible. Here the contrast between the models of Olson and Christensen (2002) and Davies et al. (2008) can be ascribed to the departure of the Rayleigh number Ra_F from criticality. In a weakly supercritical model such as that of Davies et al. (2008),

Fig. 5 Ratios G, H_{ij} of spectral Gauss coefficients of the time average field g, h_{ij} with respect to the axial dipole coefficient g_{10}. Note that Davies et al. (2008) did not report values for G22 and H22. The model at $q* = 0.3$ ($\epsilon = 0.6$ in their formalism) from Davies et al. (2008) is reported

the equatorial flux expulsion mechanism, which is the main mechanism responsible for the generation of an axial octupole, is weak, while it is considerably stronger in the study of Olson and Christensen (2002), where the departure from criticality is significantly larger.

As Figs. 4–5 suggests, the sensitivity of the numerically modelled TAF to control parameters is quite large. One parameter which has crucial implications on the TAF is the magnitude of CMB heat flow variations with respect to the mean heat flow. This has been studied in detail by Olson and Christensen (2002) and more recently by Takahashi et al. (2008). Olson and Christensen (2002) suggested that a too large degree of mantle thermal heterogeneity q^* could prevent the dynamo from working due to the existence of large, stably stratified regions disrupting the dynamo mechanism. However, Takahashi et al. (2008) showed that this phenomenon did not exist at Ekman numbers of $E = 10^{-5}$ lower than the one ($E = 3 \times 10^{-4}$) used by Olson and Christensen (2002).
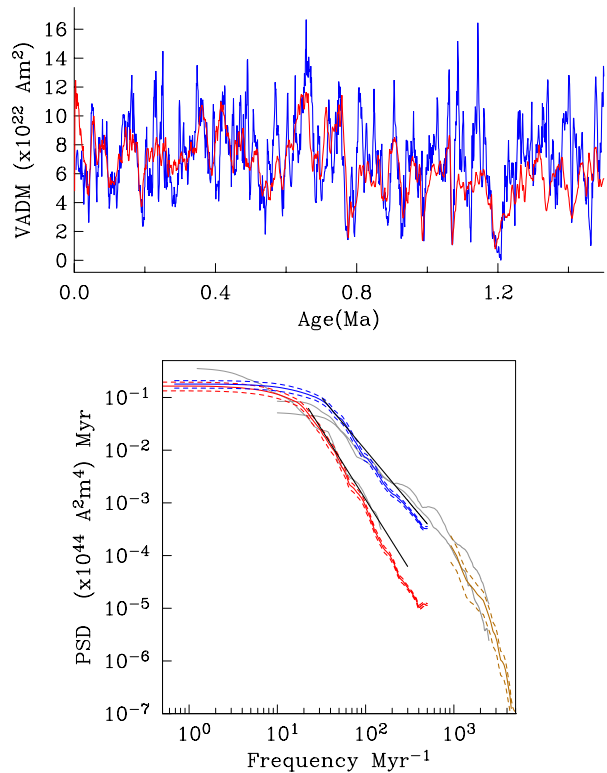
5 Dipole Moment Variations

5.1 Constraints from Relative Paleointensity, 0–2 Myr

The continuous time series available from sedimentary cores allow investigation of another aspect of paleomagnetic field behavior over the past million years or so, namely temporal variations in the dipole moment. Multiple independent time series of relative paleointensity from a variety of locations can be combined to provide regional (Laj et al. 2000; Stoner et al. 2002) or global (Valet et al. 2005; Channell et al. 2009) relative paleointensity records. Individual relative paleointensity records are stacked, averaged and scaled (using absolute paleointensity data) and under the GAD assumption an equivalent virtual axial dipole moment (VADM) calculated. Two global stacks span the past 2.0 Myr (Valet et al. 2005) or the past 1.5 Myr (Channell et al. 2009), with different studies using different approaches to establish a common chronology for the records and to scale the relative paleointensities to an absolute value. In a study in review, Ziegler (personal communication) produce a continuous time-varying paleomagnetic axial dipole moment model using a penalized maximum likelihood technique. In the paleomagnetic literature considerable attention has been focussed on the mean dipole moment over the past 1 Myr or so; as this depends on the absolute paleointensities and scalings used, we defer any such discussion to Sect. 6. However, of more interest here are the temporal variations in the dipole moment and the associated power spectrum, whose frequency dependence can be compared with predictions from numerical simulations.

Figure 6a shows an example of the evolution of VADM over the past 1.5 Myr from two global stacks: Sint-2000 (Valet et al. 2005) and PISO-1500 (Channell et al. 2009). The higher temporal resolution and greater variability in VADM of PISO-1500 compared with Sint-2000 is a consequence of the use of a larger number of high sedimentation records in the former, and the coupled relative paleointensity/oxygen isotope matching technique. Both global stacks have been scaled to have the same dipole moment for the past 800 ka (i.e., we have scaled Sint-2000 to have the same 800 kyr mean as PISO-1500). We use multi-taper direct spectral estimation (Riedel and Sidorenko 1995) to compute the corresponding power spectra for PISO-1500 and Sint-2000 (Fig. 6b) using the approach described to calculate the power spectrum for Sint-800 (Guyodo and Valet 1999) in Constable and Johnson (2005). The lower temporal resolution and muted variations in VADM of Sint-2000 as compared with PISO-1500 are evidenced in the lower amplitude and steeper fall-off with frequency of the Sint-2000 spectrum, for frequencies higher than

Fig. 6 (**a**) Sint-2000 (*red*, Valet et al. 2005) and PISO-1500 (*blue*, Channell et al. 2009), both scaled to have a 0–800 ka mean of 7.46×10^{22} A m^2, (**b**) Power spectra (*solid lines*) with 95% confidence intervals (*dashed lines*) for Sint-2000 (*red*), PISO-1500 (*blue*), millenial-scale model CALS7K.2 (*brown*, Korte et al. 2005). Also shown are the power spectra for individual records (*gray*) (VM93 Valet and Meynadier 1993), 983 (Channell et al. 1997) and 984 (Channell 1999). Note that the power spectrum for Sint-2000 is very similar to that from lower sedimentation rate records such as VM93 (the two fall almost on top of each other in the figure), where as the spectra for PISO-1500 closely tracks those of higher sedimentation records such as 983 and 984. *Black lines* indicate power spectra with slopes proportional to f^{-2} and $f^{-8/3}$

10 Myr^{-1}. The Sint-2000 spectrum essentially follows the resolution inherent in the lower sedimentation records such as that of Valet and Meynadier (1993), whose spectrum (Constable and Johnson 2005) is also shown on Fig. 6b. The power spectrum of PISO-1500 reflects the higher sedimentation records such as records 983 and 894 (Channell et al. 1997; Channell 1999)—the spectra for these individual records are also shown here as calculated in Constable and Johnson (2005). The spectrum of PISO-1500 falls off as approximately f^{-2} (as also noted by Ziegler et al. 2008 for the composite spectrum of Constable and Johnson 2005) for frequencies in the range 30 Myr^{-1} to 500 Myr^{-1}. The spectrum of Sint-2000 falls off as approximately $f^{-8/3}$ for frequencies in the range 30 My^{-1} to 100 Myr^{-1}, with possibly a steeper slope for frequencies 100–500 Myr^{-1}. The spectra of Sint-2000 and PISO-1500 reflect the spectra of the individual lower and higher sedimentation records respectively, and we can reasonably expect that any global dipole moment model derived from sediment cores to have a spectral slope bounded by those of the contributing low- and high-resolution records, providing constraints on numerical simulations of the geodynamo.

5.2 Predictions from Numerical Models

The low-frequency behavior of dipole moment time series (on time scales much larger than the time of overturn) has received little attention up to recent times, owing to the large computer resources needed to compute the long-term time series which are needed. Recently, two studies have underlined very different approaches. Olson (2007) and Driscoll and Olson (2009a) use a numerical dynamo model that is very economical in terms of control parameters, especially the Ekman number which is very high (on the order of 10^{-2}). The

Reynolds number of the flow is on the order of $Re \approx 10$, and dynamo action is ensured through the choice of a large magnetic Prandtl number $Pm > 10$ such that the magnetic Reynolds number $Rm = Re \cdot Pm$ exceeds the typical value 100 needed for dynamo action. In their model, hydrodynamic turbulence is almost absent, while magnetic turbulence is more likely to excite a broad range of time scales. In contrast, Sakuraba and Hamano (2007) use a much lower Ekman number, larger Reynolds number and a magnetic Prandtl number equal to 1. In that context, hydrodynamic turbulence is likely to play a more important role. Sakuraba and Hamano (2007) find a dipole moment power spectral density falloff $f^{-5/3}$ for $100 \, \mathrm{Myr}^{-1} < f < 300 \, \mathrm{Myr}^{-1}$ and then $f^{-11/3}$ for $300 \, \mathrm{Myr}^{-1} < f < 3000 \, \mathrm{Myr}^{-1}$. They also argue that the power $-11/3$ in dipole moment PSD is compatible with a power $-5/3$ in kinetic energy PSD, which is reminiscent of a Kolmogorov spectrum in three-dimensional isotropic and homogeneous hydrodynamic turbulence. Their corner frequency of $300 \, \mathrm{Myr}^{-1}$ is attributed to the frequency of the fundamental mode of convection. In contrast, there is no clear corner frequency in the paleomagnetic spectrum (Fig. 6), although a change in slope arises at $f > 10^3 \, \mathrm{Myr}^{-1}$. Sakuraba and Hamano (2007) ascribe the difference to either finer spatial structures in the geodynamo, or faster drift of the structures. In the long-period (low frequency) range, their dipole moment PSD exponent $-5/3$ is lower than the exponents -2 and $-8/3$ respectively obtained from Sint-2000 and PISO-1500. Olson (2007); Driscoll and Olson (2009a) find a dipole moment power spectral density falloff $f^{-7/3}$, for $3 \, \mathrm{Myr}^{-1} < f < 300 \, \mathrm{Myr}^{-1}$, and no corner frequency in that range. This exponent is more in line with Sint-2000 and PISO-1500 in the same frequency range.

The two numerical simulation studies differ in the importance given to hydrodynamic and magnetic turbulence in the simulation, which is mostly controlled by the value of the magnetic Prandtl number. The existence of a corner frequency in the study of Sakuraba and Hamano (2007) is related to the presence of hydrodynamic turbulence at frequencies where the effect of the magnetic field is not felt, because current loops dissipate on a short ohmic time. This turbulence is thus unlikely to be influenced by the magnetic field, hence its similarity with homogeneous isotropic turbulence. Such a corner frequency is not present in the simulations of Olson (2007); Driscoll and Olson (2009a) because their system does not contain hydrodynamic turbulence. In the frequency range $100 \, \mathrm{Myr}^{-1} < f < 300 \, \mathrm{Myr}^{-1}$, the difference between the exponent $-5/3$ obtained by Sakuraba and Hamano (2007) and $-7/3$ obtained by Olson (2007); Driscoll and Olson (2009a) could possibly be ascribed to how magnetic turbulence distributes the time scales in the system. As computer resources increase and make very long simulations feasible, more understanding should be gained on the influence of magnetic turbulence on the low-frequency secular variation, which is probably one of the best-constrained aspects of the paleomagnetic signal. Finally, an interesting aspect of the study of Driscoll and Olson (2009a) is to incorporate slow evolution of the thermodynamic conditions imposed by the mantle on the 10 Myr time scale, leading to the occurrence of a superchron in one of their case. This slow evolution may be seen as too fast as compared with typical mantle time scales but is a consequence of limited computer resources. In simulations reflecting the occurrence of a superchron, they reproduce an elevated ultra-low frequency plateau in the spectrum for $f < 0.5 \, \mathrm{Myr}^{-1}$, which was obtained in the paleomagnetic power spectrum of Constable and Johnson (2005).

6 Paleosecular Variation and Intensity over the Past 195 Myr

Measures of PSV from paleomagnetic data typically reported in the literature are VGP (or directional) dispersion, standard deviations in *D, I*, intensity or VADM. Here we focus on

studies of VGP dispersion from paleomagnetic data, first for the past 5 Myr (Sect. 6.1) as this is the time interval best sampled by data, and then back to 195 Myr (Sect. 6.2). As mentioned previously, paleointensity data are much more difficult to retrieve. In Sect. 6.3, we describe constraints on variations in absolute paleointensity over the past 160 Myr, in light of the experimental obstacles related to non-ideal natural magnetic carriers.

6.1 VGP Dispersion, 0–5 Myr

Measures of PSV from paleomagnetic data typically reported in the literature are VGP (or directional) dispersion, standard deviations in *D, I* and in intensity or VADM (Merrill et al. 1996). Latitudinal variations in VGP dispersion have been extensively studied (see reviews in Merrill et al. 1996; Johnson and McFadden 2007)—a general increase in VGP dispersion with latitude is observed in data sets that is roughly symmetric about the equator. Statistical models for PSV, in which the Gauss coefficients are treated as normally-distributed variables, can produce such a signal if relatively greater variance is assigned to one or more terms for which the degree, l minus the order m is odd—the so-called dipole or antisymmetric family (Kono and Tanaka 1995; Quidelleur and Courtillot 1996; Constable and Johnson 1999; Tauxe and Staudigel 2004). Models that in addition prescribe different variances for the g_l^m and h_l^m coefficients for a given degree and order can produce longitudinal variations in PSV, e.g., larger variability in intensity associated with the high latitude flux lobes (Constable and Johnson 1999).

The Pacific dipole window, or region of low secular variation beneath the Pacific, has long been a topic of debate in the paleomagnetic literature (see e.g., McElhinny et al. 1996). The observed low VGP dispersion has been argued to be an artifact due to temporal correlation among samples (McElhinny et al. 1996), and this is supported by recent calculations for Brunhes VGP dispersion in which resampling techniques are used to mitigate the uneven age distribution of Hawaiian lavas and associated age uncertainties (Johnson and Constable 2009).

6.2 VGP Dispersion, 5–195 Myr

Latitudinal variations in VGP dispersion have been inferred to vary over the past 195 Myr (McFadden et al. 1991), with lower equatorial values for, and a greater latitudinal increase in, VGP dispersion during times of low reversal frequency (e.g., Cretaceous Normal Superchron). This led to the idea that the relative contributions of the dipole and quadrupole (l-m even) families may have varied with time, in some way that reflects core-mantle boundary thermal conditions.

The background for this analysis and inferences made on core-mantle boundary processes is the well-established chronology of field reversals from the record of seafloor marine magnetic anomalies and magnetostratigraphic studies (e.g. Opdyke and Channell 1996) (Fig. 7). This chronology has been interpreted as reflecting a decrease in reversal frequency prior to the Cretaceous Normal Superchron and an increase thereafter. The long time scales of this pattern in reversal occurrence would tend to favor some role for changes in the core-mantle boundary. However, Gallet and Hulot (1997) propose that the chronology is composed of stationary and nonstationary intervals, and that superchrons occur without precursor paleomagnetic behavior. Nevertheless, since the original study of McFadden et al. (1991), a few studies have confirmed the original PSV inferences made by the authors. Tarduno et al. (2002) contributed high latitude data and summarized prior studies, arriving at a fit that agreed with the McFadden et al. (1991) trend, but with a smaller change in
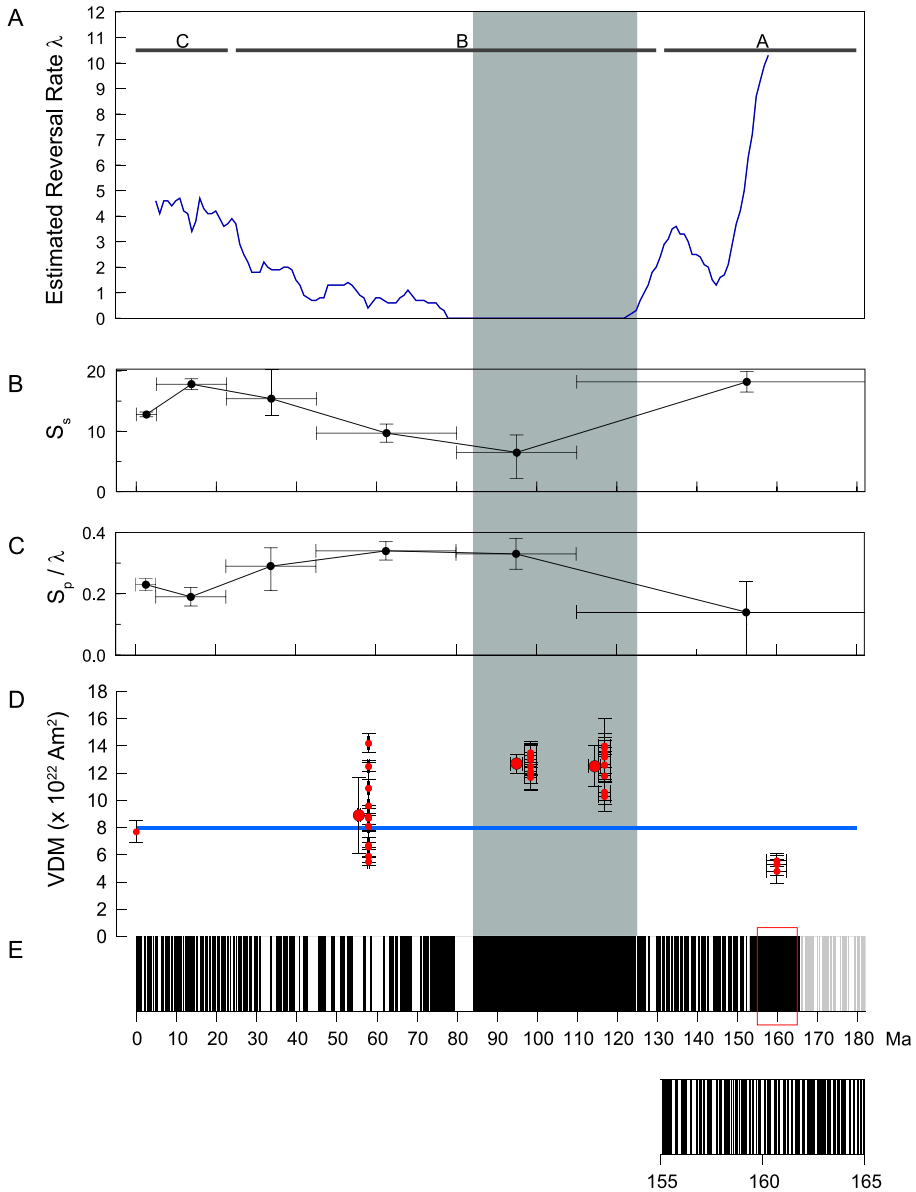
Fig. 7 Estimates of reversal rate (**A**), paleosecular variation (**B**, **C**), paleointensity (**D**) plotted versus the ge-omagnetic reversal time scale (Opdyke and Channell 1996; Gradstein et al. 2004) (**E**), where the inset shows an expanded version of the 165–155 Myr reversal chronology. Reversal rate (**A**) is shown following Tarduno and Cottrell (2005) using a 10-m.y. long sliding window and as the division of the reversal chronology into stationary (**A**, **C**) and non-stationary (**B**) intervals following Gallet and Hulot (1997). Paleosecular variation (**B**, **C**) estimates show the dipole (S_p/λ) and quadrupole (S_s) families of McFadden et al. (1991). Paleointen-sity results (**D**) are virtual dipole moments (VDMs) (*small symbols*) and their corresponding 1σ uncertainty regions from Thellier analyses of single plagioclase crystals from Tarduno and Cottrell (2005). *Large symbols* are averages of the VDMs, comprising paleomagnetic dipole moments. *Grey rectangle* highlights the Cretaceous Normal Polarity Superchron

dipole/quadrupole families between the superchron and reversing states. The high latitude data allowed Tarduno et al. (2002) to conduct a separate latitudinal test of field geometry by comparing data from the North American craton—this test confirmed the dominant dipole nature of the Cretaceous Normal Superchron field. A subsequent study by Biggin et al. (2008a) of the Cretaceous Normal Superchron and Jurassic also confirmed the inferences made by McFadden et al. (1991), but the uncertainties in PSV data for times prior to the Superchron remain large, and ripe for future studies.

6.3 Absolute Paleointensity Constraints 0–160 Myr

Tanaka et al. (1995) summarized absolute paleointensity data for rocks formed during the past 10 million years, concluding that the mean field intensity (excluding times of reversal transition) was $\sim 8.2 \times 10^{22}$ A m^2, with a standard deviation of 48.5%. The mean dipole moment over the past few Myr has been a subject of debate, because of the temporal bias in the data set toward younger units. Selkin and Tauxe (2000) claim that the value of $\sim 8 \times 10^{22}$ A m^2 is characteristic of the past 0.3 Myr, and that this is much higher than for preceding times. In fact paleointensity data bases are dominated by data from the past 50 kyr, so the temporal bias may be severe. Most of the variation reported by Tanaka et al. (1995) for the past 10 Myr probably reflects the geodynamo, but some also relates to errors related to imperfections in the natural magnetic records. This becomes an even greater problem as one seeks to describe field strength for older epochs and therefore a few words on the methods of paleointensity determination are useful before examining what these data can tell us about core-mantle boundary interactions.

The Thellier double heating method (Thellier and Thellier 1959), and its modifications advocated by Coe (1967), are generally accepted as the most robust paleointensity methods. The natural remanent magnetization (NRM) of an igneous sample is typically demagnetized by heating and cooling in a field free space. The sample is next reheated to the same temperature, but heating and cooling are done in the presence of a magnetic field. This so-called "field-on" step results in the acquisition of a partial thermoremanent magnetization (pTRM). The paired field-off and field-on steps are repeated for increments that span the entire unblocking temperature range of a rock's magnetic minerals (e.g. magnetite, up to 580°C). When the pTRM's are additive, knowledge of the NRM lost (M_{NRM}), the TRM gained (M_{TRM}), and the applied field strength (H_{lab}) allows a calculation of the past field intensity (H_{paleo}):

$$H_{paleo} = \frac{M_{NRM}}{M_{TRM}} H_{lab} \tag{12}$$

The additivity of pTRM's underlies the Thellier method and this requires that the magnetic mineral carriers to be single domain, or single-domain-like, a state that is commonly called pseudo-single domain (Stacey and Banerjee 1974). Importantly, samples must not magnetically alter during heating. If alteration occurs, the TRM data will be corrupted. This separates paleointensity studies from standard directional analyses (used for PSV studies) where samples are demagnetized in a field free environment and are thus less prone to the effects of experimentally-induced alteration. The effects of alternation can be subtle and often require extensive rock magnetic testing to detect. Also alteration tends to increase artificially increase TRM capacity, so alteration can create a bias toward paleofield underestimate (Tarduno and Smirnov 2004). For these reasons, data entries in paleointensity data bases should be scrutinized to ensure alteration is not present in any given study. Beyond the suitability of the recorder, we also must consider data density and whether sufficient time has been

averaged within each data set. We will return to this issue in the discussion of data that follows.

If correlations between field strength and reversal frequency exist on 10's of millions of years time scales, they should be best expressed during superchrons. However, in Thellier studies of whole rock samples, a clear relationship was not found, leading some to conclude that reversal rate and paleointensity are decoupled (e.g. Prévot et al. 1990). This conclusion was also reached on the basis of early analyses of submarine basaltic glass (Selkin and Tauxe 2000). Yet a prominent feature of such data syntheses is the presence of very low VDM's (e.g. $\ll 4 \times 10^{10}$ A m^2) derived for whole rocks older than 10 Myr. (Note, for VDMs, the dipole axis corresponds to that constrained by the measured paleomagnetic inclination of the site.) Cottrell and Tarduno (2000) found that paleointensity results from single plagioclase crystals hosting single-domain-like inclusions often yielded higher paleointensity results than the whole rock lava samples from which they were separated. The hypothesis suggested to explain this difference was that the whole rock paleointensity values were compromised by magnetic mineral alteration on geologic (e.g. weathering) time scales, and during laboratory treatment.

To test whether further whether single crystals might see a signal of core-mantle processes otherwise hidden by alteration in whole rocks, Tarduno et al. (2001, 2002) studied Cretaceous Normal Polarity Superchron samples and found high paleointensities ($12.5 \pm 1.4 \times 10^{22}$ A m^2 and $12.7 \pm 0.7 \times 10^{22}$ A m^2). In these studies, samples were drawn from independent cooling units spaced over a total volcanic duration of $\sim$1 m.y., ensuring considerable field averaging. Tarduno and Cottrell (2005) assayed reversal history, and found paleointensities of 8.9×10^{22} A m^2 (Tarduno and Cottrell 2005) for a time of moderate reversal frequency ($<$1 reversal/million years) at 56 Myr, and $\sim 4 \times 10^{22}$ A m^2 during a time of very high (possibly $>$10 reversals/million year) at $\sim$160 Myr. Together, these single silicate paleointensity data support an inverse relationship between reversal rate and field strength as envisioned in the landmark work of Cox (1968). As noted above, support for this relationship at the time of this review is still lacking from whole rock samples, but this may not be forthcoming because of the alteration problems. However, similar trends have been reported in subsequent paleointensity studies of submarine basaltic glass (Tauxe and Staudigel 2004). The pattern suggested by the single silicate paleointensity data support the idea that superchrons may reflect times when the nature of core-mantle boundary heat flux allows the geodynamo to operate at peak efficiency, as suggested in some numerical models (e.g. Glatzmaier et al. 1999), whereas the succeeding period of reversals may signal a less efficient dynamo with a lower dipole intensity. However, the database is small and additional studies are to be encouraged, as well as further numerical dynamo modelling efforts.

Furthermore, Tauxe and Yamazaki (2007) combined paleointensity data from different recorders (submarine basaltic glass, whole rocks, single crystal paleointensity) and concluded that there was an inverse correlation of intensity and polarity rate, in agreement with the inferences based solely on the single silicate crystal paleointensity data. Assumptions of this approach are that VDMs from any given site are independent and VDMs from different sites recorded at different times within a given polarity chron can confidently be combined to yield an average field value. The benefit of this analysis is that the number of data included is larger than that of any one data type. A possible failing beyond the assumptions above is that if systematic errors characterize data type, as discussed above for whole rock samples, field strength dispersion could be overestimated. In this regard it is interesting that Tauxe and Yamazaki (2007) conclude that field strength was greater during the Cretaceous Normal Polarity Superchron as compared to mixed polarity intervals on the basis of an amalgamation of all data types, while Tarduno et al. (2006) conclude variation was less on the basis

of single silicate results alone. Nevertheless, trends in field strength agree between the two approaches.

6.4 Predictions from Numerical Simulations

6.4.1 VGP Dispersion 0–5 Myr

Numerical dynamo models before, or slightly after the onset of reversals usually favour the dipole family over the quadrupole family in core-mantle boundary magnetic power spectra (see for instance Driscoll and Olson 2009b). Latitudinal ASD variations similar to these observed in the paleomagnetic field for the last 5 Myr are thus a robust feature in numerical geodynamo models. Kono and Roberts (2000) analyzed the dynamo models of Glatzmaier and Roberts (1995) and Sakuraba and Kono (1999) and found that the general increase of VGP dispersion with latitude is reproduced in both cases, while too small in the former case and too large in the latter case. This suggests a control parameter dependency of latitudinal ASD variations. The same parameter dependency effect seems to be visible in the models of Christensen and Olson (2003) and Wicht (2005), which, while very similar, respectively exhibit too weak and too strong ASD latitudinal variation respectively. It was proposed by Wicht (2005) that the convective vigor differences between the regions inside and outside the tangent cylinder could be held responsible for latitudinal ASD variations, in which case Ra_F is obviously a critical control parameter. Indeed the increasing effect of forcing on ASD and latitudinal ASD variations could be singled out in Christensen and Wicht (2007). While the influence of mantle control is theoretically not required to create latitudinal ASD variations, Bloxham (2000) additionally found that heterogeneous mantle control enhances ASD variations.

A heterogeneous mantle control also creates longitudinal variations in the ASD. Bloxham (2000) analyzed numerical dynamos with and without mantle control and found smaller inclination anomalies in the Pacific than elsewhere when mantle control is present. The tomographic models of Christensen and Olson (2003), which are similar to that presented in Sect. 4.2, indeed confirm that longitudinal variations can exist in the ASD of VGPs. However these longitudinal variations are small, on, the order of a degree between Hawaii and Deccan regions, which raises questions concerning their detectability in paleomagnetic data. Constable and Johnson (1999) noted that non-zonal variations in PSV may be better detected by paleomagnetic observables other than VGP dispersion, such as the standard deviations in inclination or intensity. The later analysis performed by Davies et al. (2008) concludes that their dynamo models do not show significant longitudinal variation in the ASD. However, their models typically feature less secular variation than the models run by Christensen and Olson (2003), owing mainly to the presence of a part of the magnetic field which remains permanently locked to the boundary, while the models of Christensen and Olson (2003) do not have such a locked part, but rather present a statistical preference for magnetic field features at certain longitude.

6.4.2 VGP Dispersion, 5–195 Myr

Evolving conditions at the core-mantle boundary are thought to be responsible for the occurrence of superchrons. In their study, Driscoll and Olson (2009a) propose two scenarios, one of regular evolution, marked by a decrease of Ra_F due to the gradual cooling of the Earth, and an increase in E corresponding to the tidal decrease in the Earth's rotation rate. They find that this regular evolution causes the system to evolve in a direction which is parallel, in a (Ra, E) parameter space, to the regime boundary line between non-reversing and

reversing dynamos. As the Earth's core is though to lie close to that transition (Christensen and Aubert 2006), their conclusion is that the occurrence of a superchron has to be ascribed to anomalous core forcing, for instance following the release of a localized strong mantle upwelling (Courtillot and Olson 2007). In that case, the superchron state would markedly favour the dipolar family of Gauss coefficients over the quadrupolar family (Driscoll and Olson 2009b), similarly to Fig. 7. The VGP dispersion would thus be lower at the equator with a greater latitudinal increase, as observed in the paleomagnetic field, though this result has not been systematically checked in numerical simulations. If the scenario proposed by Courtillot and Olson (2007); Driscoll and Olson (2009a) is right, then superchrons must systematically occur with a paleomagnetic warning: a slowly decreasing (on mantle time scales) reversal frequency has to be apparent prior to the superchron onset, in apparent conflict with the conclusions of Hulot and Gallet (2003), according to which superchrons would not systematically occur with such a paleomagnetic warning. This has also been recently challenged by Aubert et al. (2009), who argued that the fluctuations of Ra_F needed to trigger a superchron can be very close to fluctuations needed to shut down the dynamo altogether, thus calling for another scenario. The recent description of multiple dynamo states for a single set of control parameters (Simitev and Busse 2009) could provide an explanation: without any external influence, the dynamo could spontaneously switch from a mean dipole, non reversing state to a fluctuating dipole, reversing state on time scales that could be much longer than the longest time scales associated with core dynamics. The validity of such a scenario needs to be checked, especially the possibility of spontaneous transitions in both directions, and whether the time scales involved with the transitions between the two states can be as long as those required by the existence of superchrons over several tens of million years.

6.4.3 Absolute Paleointensity, 0–160 Myr

Reversal rates and dipole intensity are strongly correlated in numerical dynamo models. Driscoll and Olson (2009b) find a systematic decrease in the dipole intensity as Ra_F is increase above the onset of reversals, an observation which ties with the transition between a dipole-dominated, stable range and a multipolar, reversing range (Christensen and Aubert 2006). However, an aspect of the question which is troublesome for numerical dynamo models is to both reproduce the reversing character of the dynamo, while maintaining a dipolarity, or ratio between the dipole and non-dipole components of the magnetic field, of strength similar to the Earth's core. The dipole variability is also shown to increase when Ra_F is increased. In summary, the occurrence of a superchron (period of lower Ra_F if the interpretation of Courtillot and Olson 2007; Driscoll and Olson 2009a is favoured) would correspond to a stronger dipole, in agreement with Fig. 7, but also to a less variable dipole, in apparent conflict with the possible increase of the dipole variability during the CNS based on the estimate of Tauxe and Yamazaki (2007) but in agreement with the assessment of Tarduno et al. (2006).

The 0–160 Myr paleomagnetic record (based on all data types) displays a very large dispersion of virtual dipole moments (see for instance Tauxe and Yamazaki 2007), with, for instance, fluctuations from about 2×10^{22} to 20×10^{22} A m^2, occurring over short (million year) time scales. Numerical dynamo models usually exhibit dipole moment fluctuations which are typically smaller (less than the mean value), and faster (associated with core overturn time scales) (see for instance, Olson 2007), with epochs of low dipole moment representing only rare events associated with reversals. As paleointensities are obtained at different locations on the Earth's surface, an interesting question is whether a running average performed on several million years based on the total data set could indeed reflect the

actual fluctuations of the dipole intensity, in which case these could directly be compared to numerical predictions. A very strong signal remaining at these time scales would be puzzling because these are too short to represent the response of the dynamo to changing mantle conditions, and too long to be associated to dynamics related to the core overturn. Refinements in the knowledge of core-mantle boundary heat flow variations, in dynamo theory, and in variability related to paleomagnetic data type (see Sect. 6.3), would then be needed in order to make conclusions regarding the physical nature of these variations.

7 The Most Ancient Geomagnetic Field

7.1 Observations

While numerical dynamo simulations face hurdles related to limitations in computing power, efforts to obtain paleomagnetic constraints on the longest (billion year) time scales must address a formidable set of challenges posed by the incompleteness of the geologic record and later geologic events have affected the world's oldest rocks. For example, a few authors have concluded that the rate of geomagnetic reversals was low in the Precambrian (Dunlop and Yu 2004; Coe and Glatzmaier 2006) but the recording of time sequences is limited. In particular, inferences on low reversal rate made on the basis of intrusive igneous rocks may instead reflect missed reversals. One well-documented record from Siberia for the 1100 to 800 Myr interval shows numerous reversals and potential superchrons (Pavlov and Gallet 2010) reminiscent of the pattern of the last 180 million years. Investigations of early Proterozoic and Archean rocks have defined geomagnetic reversals (e.g. Strik et al. 2003; Tarduno et al. 2007) and thus there is evidence that the early field was reversing. Some progress has been made in looking at the paleomagnetic dispersion of data, but only a few time intervals—marked by widespread magmatism—allow examinations of directional dispersion versus latitude. Smirnov and Tarduno (2004) presented the first such analysis for Proterozoic-Archean rocks (∼2.5 billion years old). They concluded that the field was dominantly dipolar, and perhaps more dipolar than the 0–5 Myr field. This conclusion was supported by subsequent analysis by Biggin et al. (2008b) of the same time interval.

Here we focus on even older time scales bearing on the onset and early evolution of the field—as this is most clearly related to core processes. We further focus on paleointensity because, as discussed below, the available rock record largely precludes analyses of secular variation or reversal frequency as has been defined for Phanerozoic times. The strength of the oldest field is also important for understanding the evolution of the atmosphere and the development of a habitable planet because the geomagnetic field prevents atmospheric erosion by the solar wind (Lammer et al. 2008). These effects are beyond the scope of this review, but recent advances in defining the balance between the ancient solar wind and the magnetic field are reviewed by Tarduno et al. (2010). In fact, the geomagnetic field, and hence Earth's magnetic shield from the solar wind may be have been in place shortly after core formation. However, two hypotheses call for a delay in dynamo onset. Ozima et al. (2005) suggest a null (or very weak) field at 3.8–3.9 Gyr to explain anomalous lunar nitrogen values. They call for transport of terrestrial N from Earth's atmosphere by the solar wind and implantation on the Moon in the absence of a geomagnetic field which would otherwise inhibit N pickup. Labrosse et al. (2007), call for a delayed onset of the geodynamo, to ages as young as 4.0 to 3.4 Gyr, from a model for cooling of a dense liquid layer at the base of the early Earth's magma ocean.

While there has been intense scrutiny of Earth's oldest rocks from a host of disciplines, it is important to recognize that only a small portion of these rocks are suitable for paleomagnetic analyses. The percentage decreases greatly if we wish to investigate Mesoarchean (∼3.2 Gyr) and older times relevant for tests of the null field hypotheses. The reason for this sharp decline is the pervasiveness of low grade metamorphism—heating to temperatures of 200 to 350°C, of even in the best preserved rocks. Under these conditions natural variations in grain size and domain states of magnetic carriers translate into the variable acquisition of later magnetizations (overprints). Even populations of the most reliable magnetic recorders, single domain grains, can acquire thermoviscous magnetizations at elevated temperatures given sufficient time.

To appreciate this issue, we consider the thermal relaxation time (τ) for single domain magnetic grains, following Neél (1949, 1955) single domain theory, which can be expressed as (Dunlop and Özdemir 1997):

$$\frac{1}{\tau} = \frac{1}{\tau_0} \exp\left[-\frac{\mu_0 V M_s H_K}{2kT} \left(1 - \frac{|H_o|}{H_K} \right)^2 \right] \tag{13}$$

where τ_0 (10^{-9} s) is the interval between thermal excitations, μ_0 is the permeability of free space, V is grain volume, M_s is spontaneous magnetization, H_K is the microscopic coercive force, k is Boltzmann's constant, T is temperature, and H_0 is the applied field. The microcoercive force provides a measure of the field needed for magnetization rotation in the absence of thermal excitation (Dunlop and Özdemir 1997). This theory also can be used to derive time-temperature relationships that are useful for predicting the acquisition of later thermoviscous magnetizations. Given $H_K \gg H_0$, and relaxation times (τ_A, τ_B) representing two temperatures (T_A, T_B, respectively), we can write Pullaiah et al. (1975):

$$\frac{T_A \ln(\tau_A/\tau_0)}{M_s(T_A) H_K(T_A)} = \frac{T_B \ln(\tau_B/\tau_0)}{M_s(T_B) H_K(T_B)} \tag{14}$$

This relationship suggests that for low grade metamorphism (and a nominal reheating duration of 1 m.y.), only single domain grains with blocking temperatures greater than 400°C should be taken as firm evidence for the retention of a primary thermoremanent magnetization (Dunlop and Buchan 1977). All whole rock samples contain ensembles of multidomain, pseudo-single, single domain and superparamagnetic magnetic grains. In the case of multidomain grains, we can expect the acquisition of partial thermoviscous magnetizations up to the Curie point of the magnetic mineral in question during metamorphism due to re-equilibration of domain walls; this theory has been confirmed with detailed experiments (Dunlop and Özdemir 1997). With elevated temperatures, there is also the possibility of the acquisition of chemical remanent magnetizations, related to the growth of new magnetic minerals or the alteration of primary magnetic minerals. In this case, an original thermomagnetic remanence can be replaced by a chemical or thermochemical remanence of uncertain age and strength (Smirnov and Tarduno 2005). It is now generally accepted that prior pioneering efforts to estimate field strength on ∼3.4–3.5 billion-year-old komatiites (Hale 1987) from the Kaapvaal craton record a later chemical or thermochemical remanence related to serpentinite formation (Yoshihara and Hamano 2004). Similarly, directions reported from ∼3.4–3.5 Gyr Pilbara craton rocks (McElhinny and Senanayake 1980) appear to record a complex history of secondary remanences (Usui et al. 2009).

The magnetic properties of individual rock-forming silicate grains have been shown to be a valuable means of assessing paleointensity and directions (Cottrell and Tarduno 1999, 2000), and a means of addressing the challenges posed by the Archean geologic record

(Smirnov et al. 2003). Single silicate crystals can host magnetic carriers with single-domain-like behavior, allowing one to avoid complexities posed by the presence of multidomain grains. The silicate host tends to protect the magnetic inclusions from alternation on geologic and laboratory time scales (Tarduno 2009) and the judicious choice of silicate crystals having minimal intrinsic iron can further increase the likelihood that a primary signal is retained (Tarduno et al. 2006). Whether any given suite of silicate crystals has these characteristics can be tested using rock magnetism, and additional fields are also important to ensure that a later overprint field has not been recorded (e.g. Usui et al. 2009).

Some of the least metamorphosed Paleoarchean rocks are found in the Kaapvaal Craton of South Africa and these have been used to define the currently oldest reported paleofield values based on thermoremanent magnetizations. Paleointensity analyses of single silicate crystals (feldspar and quartz) separated from 3.2 billion-year-old plutons of the Kaapvaal craton South Africa, yield virtual dipole moments of $7.5 \pm 1.2 \times 10^{22}$ A m^2 and $6.4 \pm 2.1 \times 10^{22}$ A m^2 (or the Dalmein and Kaap Valley Plutons, respectively; Tarduno et al. 2007). Both means are within error of the present-day field strength (Fig. 8), but because the samples are from plutonic rocks that cooled slowly relative to laboratory time scales used to analyze the samples, there is a possibility that the values overestimate the true field strength. Applying corrections based on single domain theory (Halgedahl et al. 1980) results in a field value ∼50% of the modern field value. However it is possible (if not likely) that this is an overcorrection because it may not apply to pseudo-single magnetic grains (Winklhofer et al. 1997) which compose part of the silicate crystal magnetic grain populations from the Kaapvaal craton pluton examined.

Older 3.4 and 3.45 billion-year-old dacites from the Kaapvaal Craton have yielded quartz phenocrysts suitable for single crystal analyses. The paleointensity data suggest virtual dipole moments of $3.8 \pm 0.4 \times 10^{22}$ A m^2 for 3.4 Gyr samples and $5.8 \pm 0.9 \times 10^{22}$ A m^2 Gyr for 3.45 Gyr samples (Fig. 8), 48% and 73% of the modern value, respectively (Tarduno et al. 2010). Unlike paleointensity estimates from the 3.2 Gyr plutons, these paleointensity data should be less affected by cooling rates due to the relatively shallow (or surface) emplacement of the dacites. However, the shorter cooling times also suggest the data record only short time intervals, between ∼90 and ∼400 years.

Because we are considering potential null field values predicted by delayed dynamo hypotheses, it is also important to consider what a "zero" Paleoarchean field reading would appear as on Earth. For example, it is possible that a rock formed in the absence of a geodynamo could be magnetized by a field arising from solar wind interaction with Earth's early atmosphere (Tarduno et al. 2010). A model for this type of interaction for a planet lacking a dynamo is provided by Venus (Zhang et al. 2007); using this analog, the field is expected to be highly variable and at least an order of magnitude weaker than values than typify the modern terrestrial field. Therefore, the consistency and strength of the field values obtained from single crystal results from 3.2 to 3.45 Gyr rocks can be confidently interpreted as evidence for a geodynamo. Interpretation of the exact values, however, is subject to the caveats associated with cooling rates and time averaging. Below we consider these values further with respect to models of the power budget of the dynamo.

7.2 Parameter Regimes, Scaling Laws, and Modelling of the Geological Evolution of the Geodynamo

Since the pioneering work of Glatzmaier and Roberts (1995), the increase of available computer power has been used to extensively explore the parameter space which is accessible to numerical dynamo simulations. Regime diagrams have been built (Kutzner and Christensen 2002; Olson 2007; Driscoll and Olson 2009a), and scaling laws have been obtained
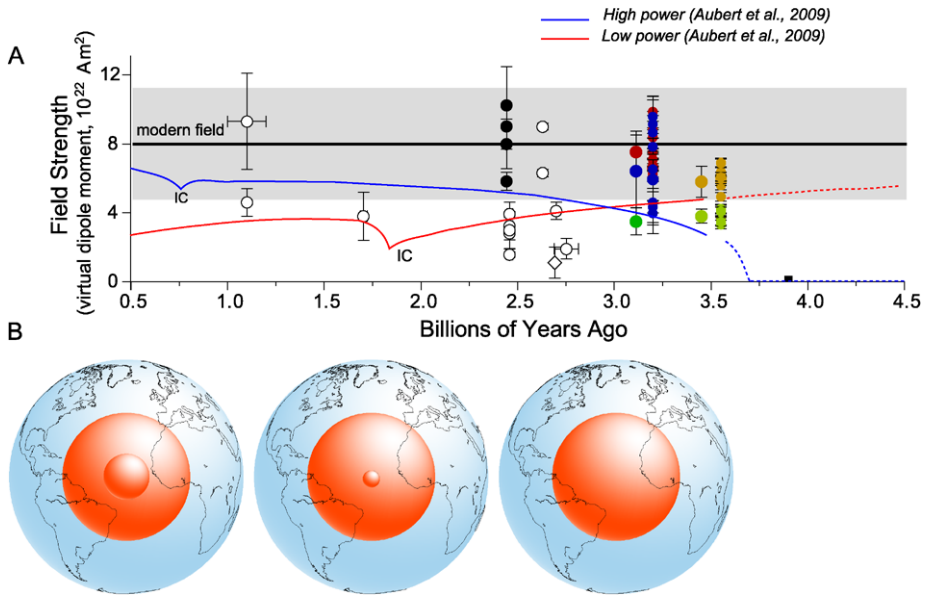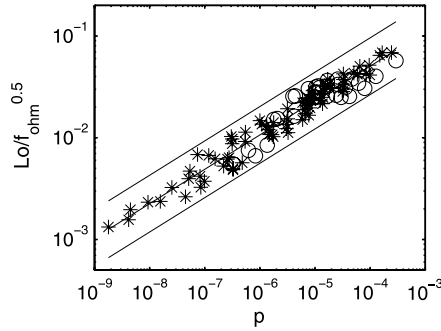
Fig. 8 (**A**) Field strength and inner core growth (see Tarduno et al. 2006 for whole rock data summary, *open symbols*). *Solid line* and *shaded area* are modern field value and typical 0–5 Myr variation, respectively. *Solid symbols* are single silicate crystal paleointensity data (*black*, Smirnov et al. 2003; *colored* Tarduno et al. 2007, 2010). *Small red* and *blue circles* are from 3.2 Gyr plutons of the Kaapvaal Craton; *large circles* are means. *Dark green circle* is mean pluton crystal value corrected for cooling rate assuming single domain theory. *Small yellow* and *light green circles* are from dacites of the Kaapvaal Craton; *large circles* are means. Null field value (*box*) at 3.9 Gyr is from hypothesis of Ozima et al. (2005). High and low power model results predict present-day core-mantle boundary heat flow rates of 11 TW and 3 TW, respectively (Aubert et al. 2009). IC marks time of inner core nucleation in each model. (**B**) Inner core growth scenario following the Aubert et al. (2009) low power model scenario

(Christensen and Tilgner 2004; Christensen and Aubert 2006; Olson and Christensen 2006) in order to evaluate the changes in dynamo characteristics with external control parameters. The increase of computer power still does not allow for extreme, more Earth-like parameter regimes to be explored, and this situation is likely to remain for some time, owing to the extreme challenges set, for example, by a decrease of 10 in the Ekman number. As the geological evolution of the dynamo can be seen as an evolution of these external control parameters (mostly a variation in the Ekman number related to the decrease of Earth's rotation rate and a change in the flux Rayleigh number related to the evolution of the Earth's core thermodynamic state), it is interesting to review the results.

As the flux Rayleigh number is increased (Kutzner and Christensen 2002), numerical dynamos transition from a stable, dipole dominated state to a reversing state, often blended with a multipole-dominated state, though there are isolated cases (Wicht 2005; Olson 2007; Driscoll and Olson 2009a) where the dynamo is reversing while multipoles do not dominate, a regime which is thought to bear the best relevance for the Earth's core. The lowest frequency associated with reversing dynamos is that of the reversal frequency, which is usually of a few cycles per million years, in agreement with the geomagnetic field (Wicht 2005). It was later recognized (Christensen and Aubert 2006) that a better parameter to locate the transition between stable and reversing numerical dynamos is a Rossby number, linked to the local inertia present in the system. In the dipole-dominated regime, the time average,

Fig. 9 Evolution of the non-dimensional Lorentz number $B_{rms}/\sqrt{\rho\mu}\,\Omega\,D$, corrected from the ohmic dissipation fraction $f_{ohm}^{1/2}$, with the non-dimensional convective power p. *Crosses* represent the points obtained by Christensen and Aubert (2006) for $\chi = 0.35$. *Circles* represent the points analyzed in Aubert et al. (2009). The full parameter space outlined in Table 1 is explored

root-mean squared magnetic field amplitude B_{rms} at the core-mantle boundary (Christensen and Aubert 2006), and the time average magnetic dipole moment (Olson and Christensen 2006) have both been shown to scale primarily with the 1/3 power of the flux Rayleigh number Ra_F, which is a proxy for the non-dimensional volumetric convective power p available to the dynamo (Aubert et al. 2009):

$$B_{rms} = f_{ohm}^{1/2}\,\sqrt{\rho\mu}\,\Omega\,D\,p^{1/3} \tag{15}$$

This scaling arises by considering a power budget of the dynamo, and the term f_{ohm} is the fraction of power dissipated through ohmic losses. It arises as a correction factor in numerical dynamos, where a sizeable part of the power is dissipated through viscous losses. The extremely low viscosity of the Earth's core, compared to the magnetic diffusivity ($Pm \approx 10^{-6}$) leads to infer $f_{ohm} \approx 1$ in the Earth's core. Figure 9 shows that the scaling is verified over a range of control parameters as expressed in Table 1. It is worth noting that diffusivities enter only marginally in a scaling such as (15), which gives credence to the mechanism underlying this scaling, as diffusivities represent the main source of discrepancy between numerical models and Earth's core in parameter space.

Can we use the information obtained from this extensive parameter space analysis to infer the geological evolution of the Earth's dynamo? Aubert et al. (2009) describe time-average dynamo characteristics as a set of scalings parametrized mostly by p. Here the time average window is long when compared to core dynamics, but instantaneous when compared to thermodynamic core evolution. Time series of p can then be obtained as an output of thermodynamic core evolution models (e.g. Labrosse 2003; Lister 2003). This opens the way to models for the geological, very long-term evolution of the dynamo.

7.3 Model Predictions Versus Data on the Longest Time Scales

We consider models presented recently by Aubert et al. (2009) for dipole strength variations with time versus available data. Two end member models of core-mantle boundary heat flow evolution are considered: one in which the present-day heat flow is predicted to be 3 TW (here called low power) and another in which the present-day value is 11 TW (here called high power). Aubert et al. (2009) concluded that owing to the power 1/3 at which the convective power p enters the dipole moment scaling, the predicted variations in mean dipole moment are small throughout Earth history. This inference is consistent with paleointensity data bases (Tauxe and Yamazaki 2007) and the fact that the oldest available values (Tarduno et al. 2007, 2010) are close to modern field values (Fig. 8). In the Aubert et al. (2009) models, the onset of inner core nucleation results in relatively small changes in

dipole moment—well within the typical range of secular variation—that are impossible to detect with present data and that will be difficult to investigate given the limitations of the rock record.

The low power model predicts values that match remarkably well the field intensity values provided by paleomagnetic analyses of single silicate crystals at 3.4–3.45 Gyr (Fig. 8). However, as discussed previously, the 3.4–3.45 Gyr data may not represent the full range of field variation due to limited time recording; this factor could account for the differences between the data and predictions of the high power model. The low and high power model end members yield identical values at ∼3 Gyr and both models match the data available from single silicate crystals at 3.2 Gyr, perhaps with moderate cooling rate corrections.

For times younger than 3.0 Gyr, the divergence in the low and high power curves bear on interesting and controversial aspects of data interpretation and core-mantle boundary heat flow. There is only one paleointensity data set available from single silicate crystals in the age range between 1.0 and 3.0 Gyr—the results of Smirnov et al. (2003) on ∼2.5 Gyr feldspars separated from dikes of the Karelian Craton (Fig. 8). These data also may not represent the full range of field variability because of limited sampling of time. Nevertheless, it is interesting that they record values similar to the present-day field whereas results from whole rocks formed during this time interval tend to yield lower field values (Fig. 8). Some have interpreted the whole rock results as evidence for a low field intensity prior to inner core growth (e.g. Macouin et al. 2003). In contrast, Smirnov and Tarduno (2005) suggest these data reflect a bias toward low field values due to the acquisition of thermochemical remanences. As noted above, the Aubert et al. (2009) models do not predict a dramatic intensity effect due to the onset of inner core growth. However, the whole rock values do agree with the low power end member model, whereas the high power end member is closer to the single silicate crystal data at 2.5 Gyr. But the data between 1 and 3.0 Gyr are very limited in number; the models should be testable with future data collections.

The low power model tends to underestimate significantly the 0–5 Myr field intensity and yields a core-mantle boundary heat flow less than the lower bound derived from seismology (7 TW; van der Hilst et al. 2007). These factors tend to favor a model closer to the high power model, which as noted above is also broadly compatible with the data on the longest time scales. Interestingly, the lower power model predicts a dynamo extending to the earliest Hadean times while the high power end member predicts a null field prior to ∼3.6 Gyr, with growth of field intensity between 3.6 and 3.5 Gyr. No data exist to investigate this interval, but tests may be possible in the future using Hadean-Archean minerals found in younger sedimentary units (Tarduno et al. 2009).

8 Summary

Paleomagnetic field behavior over long time scales contains an extraordinary wealth of information on Earth's interior dynamics and evolution. Numerical modeling aims at extracting this information from the available data, and at connecting them with other sources of geophysical information. We provide in Table 2 a summary of the various aspects of paleomagnetic field behavior and numerical simulations that have been examined in this review, as well as the main conclusions in each area. Although this field is now quite mature, the synthesis shows that a number of interesting questions remain which future efforts in paleomagnetic data acquisition, processing, modeling and numerical simulations should address.

Table 2 Summary of the properties of the long-term geomagnetic field which are covered in the present review

Property	Paleomagnetic Field	Numerical Simulations	Section
TAF over 5 million years, assuming the TAF is axisymmetric	negative inclination anomalies described in low degree spherical harmonic models by g_{20} and g_{30} terms a few percent of g_{10}	g_{20}/g_{10} weaker than inferred from observations, g_{30}/g_{10} stronger	4
TAF asymmetry between normal and reverse epochs	present between Brunhes and Matuyama, not yet well-constrained	not permitted by theory	4
Non-zonal structure in the 5 Myr TAF	inferred from lava flow directional data sets, subject of current research	robust (a consequence of mantle control)	4
Paleomagnetic power spectrum	slope -2 to $-8/3$ for $30\ \mathrm{Myr}^{-1} < f < 300\ \mathrm{Myr}^{-1}$, corner at $f \approx 1000\ \mathrm{Myr}^{-1}$, elevated plateau for $f < 1\ \mathrm{Myr}^{-1}$	spectral slope $-5/3$ to $-7/3$, corner not always present, elevated plateau associated with superchrons	5
VGP dispersion with latitude, 0–5 Myr	increases with latitude, first order signal equatorially-symmetric	similar structure, magnitude depends on forcing	5
VGP dispersion with longitude, 0–5 Myr	regional variations observed but e.g., low dispersion in Pacific due to temporal bias in data set	yes if mantle control is imposed, weak	5
VGP dispersion with latitude, 0–195 Myr	lower with greater latitudinal increase during superchrons	same	6
Paleointensity, 0–195 Myr	higher during superchrons	same	6
Relationship between reversal rate and paleointensity	paleointensity decreases if reversal rate increases	same	6
Relationship between dipole variability and chron length	debated	dipole strength is less variable during superchrons	6
Precambrian paleointensity	of similar strength as present-day	thermal dynamo with no inner core produces same paleointensity as present day	7
Geological trends in paleointensity	weak	weak owing to small exponent dependence of magnetic field on convective power	7
Signature of inner core nucleation	not yet unambiguously observed	intensity signature difficult to detect	7

Supplementary Information: Paleomagnetic Data

Paleomagnetic and paleointensity data can be found in data bases, e.g., http://www.Earthref.org, http://earth.liv.ac.uk/pint, and http://www.tsrc.uwa.edu.au/data_bases (Global Paleomagnetic Database GPMDB4-6). Such data bases are important starting points for analyses. We also urge review of the primary literature to gain an understanding of the range of geologic factors that may affect the recording fidelity of the paleomagnetic field in any given study.

References

A. Anufriev, C. Jones, A. Soward, The Boussinesq and anelastic liquid approximations for convection in the Earth's core. Phys. Earth Planet. Inter. **152**(3), 163–190 (2005). doi:10.1016/j.pepi.2005.06.004

J. Aubert, J. Aurnou, J. Wicht, The magnetic structure of convection-driven numerical dynamos. Geophys. J. Int. **172**, 945–956 (2008a). doi:10.1111/j.1365-246X.2007.03693.x

J. Aubert, H. Amit, G. Hulot, P. Olson, Thermochemical flows couple the Earth's inner core growth to mantle heterogeneity. Nature **454**(7205), 758–80 (2008b). doi:10.1038/nature07109

J. Aubert, S. Labrosse, C. Poitou, Modelling the paleo-evolution of the geodynamo. Geophys. J. Int. **179**, 1414–1428 (2009)

A. Biggin, D. van Hinsbergen, C. Langereis, G. Straathof, M. Deenen, Geomagnetic secular variation in the Cretaceous Normal Superchron and in the Jurassic. Phys. Earth Planet. Inter. **169**, 3–19 (2008a)

A.J. Biggin, G.H.M.A. Strik, C.G. Langereis, Evidence for a verylong-term trend in geomagnetic secular variation. Nat. Geosci. **1**, 395–398 (2008b)

J. Bloxham, The effect of thermal core-mantle interactions on the palaeomagnetic secular variation. Philos. Trans. R. Soc. Lond. **358**(1768), 1171–1179 (2000)

J. Bloxham, Time-independent and time-dependent behaviour of high-latitude flux bundles at the core-mantle boundary. Geophys. Res. Let. **29**(18), 1854 (2002)

J. Bloxham, D. Gubbins, Thermal core-mantle interactions. Nature **325**, 511–513 (1987)

D.G.J. Bloxham, A. Jackson, Geomagnetic secular variation. Philos. Trans. R. Soc. Lond. A **329**, 415–502 (1989)

C. Bouligand, G. Hulot, A. Khokhlov, G.A. Glatzmaier, Statistical paleomagnetic field modeling and dynamo numerical simulation. Geophys. J. Int. **161**, 603–626 (2005)

S.I. Braginsky, P.H. Roberts, Equations governing convection in Earths core and the geodynamo. Geophys. Astrophys. Fluid Dyn. **79**(1–4), 1–97 (1995)

J.E.T. Channell, Geomagnetic paleointensity and directional secular variation at Ocean Drilling Program (ODP) Site 984 (Bjorn Drift) since 500 ka: Comparisons with ODP Site 983 (Gardar Drift). J. Geophys. Res. **104**(B10), 22937–22951 (1999)

J.E.T. Channell, D.A. Hodell, B. Lehman, Relative geomagnetic paleointensity and ^{18}O at ODP Site 983 (Gardar Drift, North Atlantic) since 350 ka. Earth Planet. Sci. Lett. **153**, 103–118 (1997)

J.E.T. Channell, C. Xuan, D.A. Hodell, Stacking paleointensity and oxygen isotope data for the last 1.5 Myr (PISO-1500). Earth Planet. Sci. Lett. **283**(1–4), 14–23 (2009). doi:10.1016/j.epsl.2009.03.012

U. Christensen, J. Aubert, Scaling properties of convection-driven dynamos in rotating spherical shells and application to planetary magnetic fields. Geophys. J. Int. **117**, 97–114 (2006). doi:10.1111/j.1365-246X.2006.03009.x

U. Christensen, P. Olson, Secular variation in numerical geodynamo models with lateral variations of boundary heat flux. Phys. Earth Planet. Inter. **138**, 39–54 (2003). doi:10.1016/S0031-9201(03)00064-5

U. Christensen, A. Tilgner, Power requirement of the geodynamo from ohmic losses in numerical and laboratory dynamos. Nature **429**, 169–171 (2004). doi:10.1038/nature02508

U.R. Christensen, J. Wicht, *Treatise of Geophysics. 8-core Dynamics*, vol. 8 (Elsevier, Amsterdam, 2007)

U.R. Christensen, J. Aubert, F.H. Busse, P. Cardin, E. Dormy, S. Gibbons, G.A. Glatzmaier, Y. Honkura, C.A. Jones, M. Kono, M. Matsushima, A. Sakuraba, F. Takahashi, A. Tilgner, J. Wicht, K. Zhang, A numerical dynamo benchmark. Phys. Earth Planet. Inter. **128**, 25–34 (2001)

U.R. Christensen, J. Aubert, G. Hulot, Conditions for earth-like geodynamo models. Earth. Plan. Sci. Lett. (2010). doi:10.1016/j.epsl.2010.06.009

B. Clement, Geographic distribution of transitional vgps: evidence for non-zonal equatorial symmetry during the matuyama–brunhes geomagnetic reversal. Earth Planet. Sci. Lett. **104**, 48–58 (1991)

R. Coe, The determination of paleointensities of the earth's magnetic field with emphasis on mechanisms which could cause non-ideal behaviour in Thelliers method. J. Geomagn. Geoelectr. **19**, 157–179 (1967)

R.S. Coe, G.A. Glatzmaier, Symmetry and stability of the geomagnetic field. Geophys. Res. Lett. **33**(21) (2006). doi:10.1029/2006GL027903

C.G. Constable, C.L. Johnson, Anisotropic paleosecular variation models: Implications for geomagnetic observables. Phys. Earth Planet. Inter. **115**, 35–51 (1999)

C. Constable, C. Johnson, A paleomagnetic power spectrum. Phys. Earth Planet. Inter. **153**(1–3, Sp. Iss. SI), 61–73 (2005). doi:10.1016/j.pepi.2005.03.015

S. Costin, B. Buffett, Preferred reversal paths caused by a heterogeneous conducting layer at the base of the mantle. J. Geophys. Res. **109** (2005). doi:10.1029/2003002853

R.D. Cottrell, J.A. Tarduno, Geomagnetic paleointensity derived from single plagioclase crystals. Earth Planet. Sci. Lett. **169**, 1–5 (1999)

R.D. Cottrell, J.A. Tarduno, In search of high-fidelity geomagnetic paleointensities; a comparison of single plagioclase crystal and whole rock Thellier-Thellier analyses. J. Geophys. Res. **105**, 23579–23594 (2000)

V. Courtillot, P. Olson, Mantle plumes link magnetic superchrons to phanerozoic mass depletion events. Earth. Planet. Sci. Let. **260**(3–4), 495–504 (2007). doi:10.1016/j.epsl.2007.06.003

A. Cox, Lengths of geomagnetic polarity intervals. J. Geophys. Res. **73**, 3247–3260 (1968)

A. Cox, R. Doell, Review of paleomagnetism. Bull. Geol. Soc. Am. **71**, 645–768 (1960)

A. Cox, R. Doell, Long period variations of the geomagnetic field. Bull. Seism. Soc. Am., 2243–2270 (1964)

C.J. Davies, D. Gubbins, A.P. Willis, P.K. Jimack, Time-averaged paleomagnetic field and secular variation: Predictions from dynamo solutions based on lower mantle seismic tomography. Phys. Earth Planet. Inter. **169**(1–4, Sp. Iss. SI), 194–203 (2008). doi:10.1016/j.pepi.2008.07.021

P. Driscoll, P. Olson, Polarity reversals in geodynamo models with core evolution. Earth. Planet. Sci. Let. **282**(1–4), 24–33 (2009a). doi:10.1016/j.epsl.2009.02.017

P. Driscoll, P. Olson, Effects of buoyancy and rotation on the polarity reversal frequency of gravitationally-driven numerical dynamos. Geophys. J. Int. **178**, 1337–1350 (2009b)

D.J. Dunlop, K.L. Buchan, Thermal remagnetization and the paleointensity record of metamorphic rocks. Phys. Earth Planet. Inter. **13**, 325–331 (1977)

D. Dunlop, O. Özdemir, *Rock Magnetism: Fundamentals and Frontiers* (Cambridge University Press, Cambridge, 1997)

D.J. Dunlop, Y. Yu, Intensity and polarity of the geomagnetic field during precambrian time, in *Timescales of the Paleomagnetic Field*, ed. by J. Channell, D. Kent, W. Lowrie, J. Meert. Geophs. Monogr. Ser., vol. 145 (AGU, Washington, 2004), pp. 85–100

D.A.D. Evans, Proterozoic low orbital obliquity and axial-dipolar geomagnetic field from evaporite palaeo-latitudes. Nature **444**(7115), 51–55 (2006). doi:10.1038/nature05203

Y. Gallet, G. Hulot, Stationary and non-stationary behavior within the geomagnetic polarity timescale. Geophys. Res. Lett. **24**, 1875–1878 (1997)

G.A. Glatzmaier, P.H. Roberts, A three dimensional self consistent computer simulation of the geomagnetic field reversal. Nature **377**, 203–209 (1995)

G.A. Glatzmaier, R.S. Coe, L. Hongre, P.H. Roberts, The role of the Earth's mantle in controlling the frequency of geomagnetic reversals. Nature **401**(6756), 885–890 (1999)

F.M. Gradstein, J.G. Ogg, A.G. Smith (eds.), *A Geologic Time Scale 2004* (Cambridge University Press, Cambridge, 2004)

D. Gubbins, J. Bloxham, Geomagnetic field analysis—iii. magnetic fields on the core-mantle boundary. Geophys. J. Int. **80**, 695–713 (1985)

D. Gubbins, P. Kelly, Persistent patterns in the geomagnetic field over the past 2.5 Myr. Nature **365**, 829–832 (1993)

D. Gubbins, M. Richards, Coupling of the core dynamo and mantle: thermal or topographic? Geophys. Res. Lett. **365**, 1521–1524 (1986)

D. Gubbins, A.P. Willis, B. Sreenivasan, Correlation of earth's magnetic field with lower mantle thermal and seismic structure. Phys. Earth Planet. Inter. **162**(3–4), 256–260 (2007)

Y. Guyodo, J. Valet, Global changes in geomagnetic intensity during the past 800 thousand years. Nature **399**, 249–252 (1999)

C.J. Hale, Paleomagnetic data suggest link between the Archean-Proterozoic boundary and inner-core nucleation. Nature **329**(6136), 233–237 (1987)

S.L. Halgedahl, R. Day, M. Fuller, The effect of cooling rate on the intensity of weak-field trm in single-domain magnetite. J. Geophys. Res. **85**, 3690–3698 (1980)

R. Hide, On the Earth's core-mantle interface. Q. J. R. Meterol. Soc. **96**, 579–590 (1970)

J. Hospers, Remanent magnetism of rocks and the history of the geomagnetic field. Nature **168**, 1111–1112 (1951)

G. Hulot, Y. Gallet, Do superchrons occur without any palaeomagnetic warning? Earth Planet. Sci. Lett. **210**(1–2), 191–201 (2003). doi:10.1016/S0012-821X(03)00130-4

G. Hulot, C. Eymin, B. Langlais, M. Mandea, N. Olsen, Small-scale structure of the geodynamo inferred from Oersted and Magsat satellite data. Nature **416**, 620–623 (2002)

A. Jackson, A.R.T. Jonkers, M.R. Walkers, Four centuries of geomagnetic secular variation from historical records. Philos. Trans. R. Soc. A **358**, 957–990 (2000)

C. Johnson, C. Constable, The time averaged geomagnetic field as recorded by lava flows over the past 5 Myr. Geophys. J. Int. **112**, 489–519 (1995)

C.L. Johnson, C.G. Constable, The time-averaged geomagnetic field: Global and regional biases for 0–5 ma. Geophys. J. Int. **131**, 643–666 (1997)

C. Johnson, C.G. Constable, Biases in time-averaged field and paleosecular variation studies. EOS Trans. AGU, Fall Meeting Suppl. **90**(52), 23–0775 (2009)

C. Johnson, P. McFadden, *Treatise on Geophysics, Geomagnetism, Time-Averaged Field and Paleosecular Variation*, vol. 5 (Elsevier, Amsterdam, 2007)

C.L. Johnson, C. Constable, L. Tauxe, R. Barendregt, L. Brown, R. Coe, P. Layer, V. Mejia, N. Opdyke, B. Singer, H. Staudigel, D. Stone, Recent investigations of the 0–5 ma geomagentic field recorded by lava flows. Geochem. Geophys. Geosyst. **9**(4) (2008). doi:10.1029/2007GC001696

P. Kelly, D. Gubbins, The geomagnetic field over the past 5 million years. Geophys. J. Int. **128**(2), 315–330 (1997)

D. Kent, M. Smethurst, Shallow bias of paleomagnetic inclinations in the Paleozoic and Precambrian. Earth Planet. Sci. Lett. **160**(3–4), 391–402 (1998)

M. Kono, P.H. Roberts, Recent geodynamo simulations and observations of the geomagnetic field. Rev. Geophys. **40**(4), 1013 (2000)

M. Kono, H. Tanaka, Mapping the gauss coefficients to the pole and the models of paleosecular variation. J. Geomagn. Geoelectr. **47**, 115–130 (1995)

M. Korte, A. Genevey, C. Constable, U. Frank, E. Schnepp, Continuous geomagnetic field models for the past 7 millenia: 1. A new global data compilation. Geochem. Geophys. Geosyst. **6** (2005)

C. Kutzner, U. Christensen, From stable dipolar to reversing numerical dynamos. Phys. Earth Planet. Inter. **131**, 29–45 (2002)

S. Labrosse, Thermal and magnetic evolution of the Earth's core. Phys. Earth Planet. Inter. **140**, 127–143 (2003)

S. Labrosse, J.W. Hernlund, N. Coltice, A crystallizing dense magma ocean at the base of the Earth's mantle. Nature **450**(7171), 866–869 (2007)

C. Laj, A. Mazaud, A.R. Weeks, M. Fuller, E. Herrerobervera, Geomagnetic reversal paths. Nature **351**(6326), 447 (1991)

C. Laj, C. Kissel, A. Mazaud, J. Channell, J. Beer, North Atlantic palaeointensity stack since 75 ka (NAPIS-75) and the duration of the Laschamp event. Philos. Trans. R. Soc. Lond. **358**(1768), 1009–1025 (2000)

H. Lammer, J. Kasting, E. Chassefière, R. Johnson, Yu.N. Kulikov, F. Tian, Atmospheric escape and evolution of terrestrial planets and satellites. Space Sci. Rev. **139**, 399–436 (2008)

R.L. Larson, P. Olson, Mantle plumes control magnetic reversal frequency. Earth Planet. Sci. Lett. **107**(3–4), 437–447 (1991). doi:10.1016/0012-821X(91)90091-U

K. Lawrence, C. Constable, C.L. Johnson, Paleosecular variation and the average geomagnetic field at ±20° latitude. Geochem. Geophys. Geosyst. **7** (2006). doi:10.1029/2005GC001181

J.R. Lister, Expressions for the dissipation driven by convection in the Earth's core. Phys. Earth Planet. Inter. **140**(1–3), 145–158 (2003). doi:10.1016/j.pepi.2003.07.007

J.R. Lister, B.A. Buffett, The strength and efficiency of thermal and compositional convection in the geodynamo. Phys. Earth Planet. Inter. **91**(1–3), 17–30 (1995)

M. Macouin, J. Valet, J. Besse, K. Buchan, R. Ernst, M. LeGoff, U. Scharer, Low paleointensities recorded in 1 to 2.4 Ga Proterozoic dykes, Superior Province, Canada. Earth Planet. Sci. Lett. **213**, 79–95 (2003)

G. Masters, G. Laske, H. Bolton, A. Dziewonski, The relative behavior of shear velocity, bulk sound speed, and compressional velocity in the mantle: Implications for chemical and thermal structure, in *Earth's Deep Interior*, vol. 117, ed. by S. Karato, A. Forte, R.C. Liebermann, M. G., L. Stixrude (AGU Monograph, Washington, 2000)

M.W. McElhinny, W.E. Senanayake, Paleomagnetic evidence for the existence of the geomagnetic field 3.5 ga ago. J. Geophys. Res. **85**, 3523–3528 (1980)

M. McElhinny, P. McFadden, R. Merrill, The myth of the Pacific dipole window. Earth Planet. Sci. Lett. **143**(1–4), 13–22 (1996)

P.L. McFadden, R.T. Merrill, M.W. McElhinny, S.H. Lee, Reversals of the earths magnetic-field and temporal variations of the dynamo families. J. Geophys. Res. **96**(B3), 3923–3933 (1991)

R.T. Merrill, M.W. McElhinny, Anomalies in the time averaged paleomagnetic field and their implications for the lower mantle. Rev. Geophys. **15**, 309–323 (1977)

R. Merrill, P. McFadden, The geomagnetic axial dipole field assumption. Phys. Earth Planet. Inter. **139**(3–4), 171–185 (2003). doi:10.1016/j.pepi.2003.07.016

R.T. Merrill, P.L. McFadden, *The Magnetic Field of the Earth: Paleomagnetism, the Core and the Deep Mantle* (Academic Press, San Diego, 1996)

L. Neél, Théorie du traînage magneétique des ferromagnéétiques en grains fins avec application aux terres cuites. Ann. Géophys. **5**, 99–136 (1949)

L. Neél, Some theoretical aspects of rock magnetism. Philos. Mag. Suppl. **4**, 191–243 (1955)

F. Nimmo, *Treatise on Geophysics, Core Dynamics, Energetics of the Core*, vol. 8 (Elsevier, Amsterdam, 2007)

P. Olson, Gravitational dynamos and the low frequency geomagnetic secular variation. Proc. Natl. Acad. Sci. **104**(51), 20159–20166 (2007). doi:10.1073/pnas.0709081104

P. Olson, U. Christensen, The time averaged magnetic field in numerical dynamos with non-uniform boundary heat flow. Geophys. J. Int. **151**, 809–823 (2002)

P. Olson, U.R. Christensen, Dipole moment scaling for convection-driven planetary dynamos. Earth Planet. Sci. Let. **250**(3–4), 561–571 (2006). doi:10.1016/j.epsl.2006.08.008

P. Olson, U. Christensen, G.A. Glatzmaier, Numerical modelling of the geodynamo: mechanisms of field generation and equilibration. J. Geophys. Res. **104**(B5), 10383–10404 (1999)

N. Opdyke, J. Channell, *Magnetic Stratigraphy* (Academic Press, San Diego, 1996)

N.D. Opdyke, K.W. Henry, A test of the dipole hypothesis. Earth Planet. Sci. Lett. **6**, 139–151 (1969)

M. Ozima, K. Seki, N. Terada, Y.N. Miura, F.A. Podosek, H. Shinagawa, Terrestrial nitrogen and noble gases in lunar soils. Nature **436**, 655–659 (2005)

V. Pavlov, Y. Gallet, Variations in geomagnetic reversal frequency during the Earth's middle age. Geochem. Geophys. Geosyst. **11**, 01710 (2010)

M. Prévot, M.E.M. Derder, M. McWilliams, J. Thompson, Intensity of the Earth's magnetic field: Evidence for a Mesozoic dipole low. Earth Planet. Sci. Lett. **97**, 129–139 (1990)

G. Pullaiah, E. Irving, K.L. Buchan, D.J. Dunlop, Magnetization changes caused by burial and uplift. Earth Planet. Sci. Lett. **28**, 133–143 (1975)

X. Quidelleur, V. Courtillot, On low degree spherical harmonic models of paleosecular variation. Phys. Earth Planet. Inter. **95**, 55–77 (1996)

K. Riedel, A. Sidorenko, Minimum bias multiple taper spectral estimation. IEEE Trans. Signal Process. **43**, 188–195 (1995)

A. Sakuraba, Y. Hamano, Turbulent structure in Earth's fluid core inferred from time series of geomagnetic dipole moment. Geophys. Res. Lett. **34**(15) (2007). doi:10.1029/2007GL029898

A. Sakuraba, M. Kono, Effect of the inner core on the numerical solution of the magnetohydrodynamic dynamo. Phys. Earth Planet. Inter. **111**(1–2), 105–121 (1999)

P. Selkin, L. Tauxe, Long-term variations in palaeointensity. Philos. Trans. R. Soc. Lond. A **358**(1768), 1065–1088 (2000)

R.D. Simitev, F.H. Busse, Bistability and hysteresis of dipolar dynamos generated by turbulent convection in rotating spherical shells. EPL **85**(1) (2009). doi:10.1209/0295-5075/85/19001

A. Smirnov, J. Tarduno, Secular variation of the Late Archean Early Proterozoic geodynamo. Geophys. Res. Lett. **31**(16) (2004). doi:10.1029/2004GL020333

A. Smirnov, J. Tarduno, Thermochemical remanent magnetization in Precambrian rocks: Are we sure the geomagnetic field was weak? J. Geophys. Res. **110**, 06103 (2005). doi:10.1029/2004JB003445

A.V. Smirnov, J.A. Tarduno, B.N. Pisakin, Paleointensity of the early geodynamo (2.45 Ga) as recorded in Karelia; a single-crystal approach. Geology **31**, 415–418 (2003)

B. Sreenivasan, D. Gubbins, Dynamos with weakly convecting outer layers: implications for core-mantle boundary interaction. Geophys. Astrophys. Fluid Dyn. **102**(4), 395–407 (2008). doi:10.1080/03091920801900047

F.D. Stacey, S.K. Banerjee, *The Physical Principles of Rock Magnetism* (Elsevier, Amsterdam, 1974)

J. Stoner, C. Laj, J. Channell, C. Kissel, South Atlantic and North Atlantic geomagnetic paleointensity stacks (0–80 ka): implications for inter-hemispheric correlation. Q. Sci. Rev. **21**(10), 1141–1151 (2002)

G. Strik, T. Blake, T. Zegers, S. White, C. Langereis, Palaeomagnetism of flood basalts in the Pilbara Craton, Western Australia: Late Archaean continental drift and the oldest known reversal of the geomagnetic field. J. Geophys. Res. **108**(B12) (2003). doi:10.1029/2003JB002475

F. Takahashi, H. Tsunakawa, M. Matsushima, N. Mochizuki, Y. Honkura, Effects of thermally heterogeneous structure in the lowermost mantle on the geomagnetic field strength. Earth Planet. Sci. Lett. **272**(3–4), 738–746 (2008). doi:10.1016/j.epsl.2008.06.017

H. Tanaka, M. Kono, H. Uchimura, Some global features of paleointensity in geological time. Geophys. J. Int. **120**, 97–102 (1995)

J.A. Tarduno, Geodynamo history preserved in single silicate crystals; origins and long-term mantle control. Elements **5**, 217–222 (2009)

J.A. Tarduno, R.D. Cottrell, Dipole strength and variation of the time-averaged reversing and nonreversing geodynamo based on Thellier analyses of single plagioclase crystals. J. Geophys. Res. **110**, 11101 (2005)

J.A. Tarduno, A.V. Smirnov, The paradox of lowfield values and the long-term history of the geodynamo, in *Timescales of the Paleomagnetic Field*, ed. by J. Channell, D. Kent, W. Lowrie, J. Meert. Geophys. Monogr. Ser., vol. 145 (AGU, Washington, 2004), pp. 75–84

J.A. Tarduno, R.D. Cottrell, A.V. Smirnov, High geomagnetic intensity during the mid-cretaceous from thellier analyses of single plagioclase crystals. Science **291**, 1779–1783 (2001)

J.A. Tarduno, R.D. Cottrell, A.V. Smirnov, The Cretaceous superchron geodynamo: Observations near the tangent cylinder. Proc. Natl. Acad. Sciences **99**, 14020–14025 (2002)

J.A. Tarduno, R.D. Cottrell, A.V. Smirnov, The paleomagnetism of single silicate crystals; recording geomagnetic field strength during mixed polarity intervals, superchrons, and inner core growth. Rev. Geophys. **44**, 1002 (2006)

J.A. Tarduno, R.D. Cottrell, M.K. Watkeys, D. Bauch, Geomagnetic field strength 3.2 billion years ago recorded by single silicate crystals. Nature **446**(7136), 657–660 (2007). doi:10.1038/nature05667

J.A. Tarduno, J. Nelson, R.D. Cottrell, M.K. Watkeys, Exploring the magnetic sands of time: using zircons and other sedimentary detritus to understand the early geodynamo. Eos Trans. AGU **90**(22) (2009). Jt. Assem. Suppl., Abstract GP21A-03

J.A. Tarduno, R.D. Cottrell, M.K. Watkeys, A. Hofmann, P.V. Doubrovine, E.E. Mamajek, D. Liu, D.G. Sibeck, L.P. Neukirch, Y. Usui, Geodynamo, solar wind, and magnetopause 3.4 to 3.45 billion years ago. Science **327**(5970), 1238–1240 (2010). doi:10.1126/science.1183445. http://www.sciencemag.org/cgi/content/abstract/327/5970/1238

L. Tauxe, D. Kent, A simplified statistical model for the geomagnetic field and the detection of shallow bias in paleomagnetic inclinations: Was the ancient magnetic field dipolar? in *Timescales of the Paleomagnetic Field*, vol. 145, ed. by J.E.T. Channell, D.V. Kent, W. Lowrie, J.G. Meert (AGU, Washington, 2004), pp. 101–115

L. Tauxe, H. Staudigel, Strength of the geomagnetic field in the Cretaceous Normal Superchron: New data from submarine basaltic glass of the Troodos Ophiolite. Geochem. Geophys. Geosyst **5**, 02–06 (2004)

L. Tauxe, T. Yamazaki, Paleointensities, in *Treatise on Geophysics. 5-Geomagnetism*, ed. by G. Schubert (Elsevier, Amsterdam, 2007)

E. Thellier, O. Thellier, Sur l'intensité du champ magnétique terrestre dans le passé historique et géologique. Ann. Geophys. **15**, 285–376 (1959)

T. Torsvik, R. Van der Voo, Refining Gondwana and Pangea palaeogeography: estimates of Phanerozoic non-dipole (octupole) fields. Geophys. J. Int. **151**(3), 771–794 (2002)

Y. Usui, J.A. Tarduno, M. Watkeys, A. Hofmann, R.D. Cottrell, Evidence for a 3.45-billion-year-old magnetic remanence; hints of an ancient geodynamo from conglomerates of South Africa. Geochem. Geophys. Geosyst. **10**, 09–07 (2009)

J.P. Valet, Time variations in geomagnetic intensity. Rev. Geophys. **41**(1), 1004 (2003)

J.P. Valet, L. Meynadier, Geomagnetic field intensity and reversals during the past four million years. Nature **336**, 234–238 (1993)

J. Valet, L. Meynadier, Y. Guyodo, Geomagnetic dipole strength and reversal rate over the past two million years. Nature **435**(7043), 802–805 (2005). doi:10.1038/nature03674

R. van der Hilst, M.V. De Hoop, P. Wang, S.H. Shim, P. Ma, L. Tenorio, Seismostratigraphy and thermal structure of Earth's core-mantle boundary region. Science **315**, 1813–1817 (2007)

R. Van der Voo, T. Torsvik, Evidence for late Paleozoic and Mesozoic non-dipole fields provides an explanation for the Pangea reconstruction problems. Earth Planet. Sci. Lett. **187**(1–2), 71–81 (2001)

J. Wicht, Inner-core conductivity in numerical dynamo simulations. Phys. Earth Planet. Inter. **132**, 281–302 (2002)

J. Wicht, Palaeomagnetic interpretation of dynamo simulations. Geophys. J. Int. **162**, 371–380 (2005). doi:10.1111/j.1365-246X.2005.02665.x

A.P. Willis, B. Sreenivasan, D. Gubbins, Thermal core-mantle interaction: Exploring regimes for 'locked' dynamo action. Phys. Earth Planet. Int. **165**(1–2), 83–92 (2007). doi:10.1016/j.pepi.2007.08.002

R. Wilson, Permanent aspects of the earth's non-dipole magnetic field over Upper Tertiary times. Geophys. J. **19**, 417–439 (1970)

M. Winklhofer, K. Fabian, F. Heider, Magnetic blocking temperatures of magnetite calculated with a three-dimensional micromagnetic model. J. Geophys. Res. **102**, 22695–22709 (1997)

A. Yoshihara, Y. Hamano, Paleomagnetic constraints on the Archean geomagnetic field intensity obtained from komatiites of the Barberton and Belingwe greenstone belts, South Africa and Zimbabwe. Precambrian Res. **131**, 111–142 (2004)

T. Zhang, et al., Little or no solar wind enters Venus' atmosphere at solar minimum. Nature **450**, 654–656 (2007)

L.B. Ziegler, C.G. Constable, C.L. Johnson, Testing the robustness and limitations of 0–1 Ma absolute paleointensity data. Phys. Earth Planet. Inter. **170**(1–2), 34–45 (2008). doi:10.1016/j.pepi.2008.07.027